J. Fluid Mech. (2023), *vol*. 962, A40, doi:10.1017/jfm.2023.259

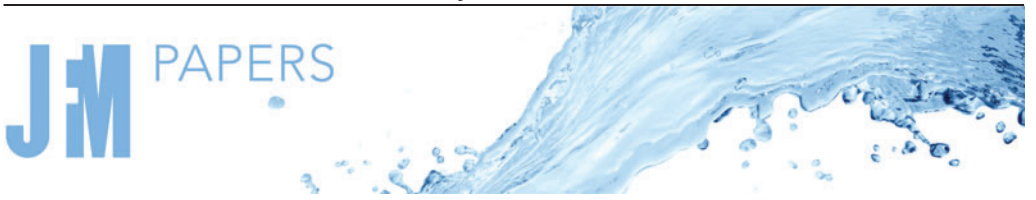

Buoyancy-driven bubbly flows: role of meso-scale structures on the relative motion between phases in bubble columns operated in the heterogeneous regime

Y. Mezui[1], **M. Obligado**[1] **and A. Cartellier**[1],†

[1]Université Grenoble Alpes, CNRS, Grenoble-INP, LEGI, F-38000 Grenoble, France

(Received 5 October 2022; revised 11 February 2023; accepted 13 March 2023)

The hydrodynamics of bubble columns in the heterogeneous regime is investigated from experiments with bubbles at large particle Reynolds numbers and without coalescence. The void fraction field ε at small scales, analysed with Voronoï tessellations, corresponds to a random Poisson process (RPP) in homogeneous conditions but it significantly differs from an RPP in the heterogeneous regime. The distance to an RPP allows identifying meso-scale structures, namely clusters, void regions and intermediate regions. A series of arguments demonstrate that the bubble motion is driven by the dynamics of these structures. Notably, bubbles in clusters (respectively in intermediate regions) are moving up faster, up to 3.5 (respectively 2) times the terminal velocity, than bubbles in void regions whose absolute velocity equals the mean liquid velocity. In addition, the mean unconditional relative velocity of bubbles is recovered from mean relative velocities conditional to meso-scale structures, weighted by the proportion of bubbles in each structure. Assuming buoyancy–inertia equilibrium for each structure, the relative velocity is related to the characteristic size and concentration of meso-scale structures. By considering the latter quantity's values at large gas superficial velocities, a cartoon of the internal flow structure is proposed. Arguments are proposed to help understanding why the relative velocity scales as $(gD\varepsilon)^{1/2}$ (with D the column's diameter and g gravity's acceleration). The proposed cartoon seems consistent with a fast-track mechanism that, for the moderate Rouse numbers studied, leads to liquid velocity fluctuations proportional to the relative velocity. The potential impact of coalescence on the above analysis is also commented.

Key words: gas/liquid flow, multiphase flow

† Email address for correspondence: alain.cartellier@cnrs.fr

1. Introduction

In bubble columns, gas is injected at the bottom of a vertical cylinder filled with liquid. Such systems are commonly employed as reactors (for chemical or biochemical transformations), mixers (metallurgy) and separators (flotation), among several other applications. For a low enough gas flow rate, bubbles are uniformly distributed over the column cross-section and gently rise up to the free surface. A characteristic of this so-called homogeneous regime is the linear increase of the void fraction ε with the gas superficial velocity V_{sg} (the latter is defined as the injected gas flow rate divided by the column cross-section). The apparent rise velocity, evaluated as V_{sg}/ε, is nearly constant in this regime, and its magnitude is of the order of the bubbles' terminal velocity U_T. When increasing the inlet gas flow rate above some threshold, the flow becomes non-uniform, and a mean recirculation settles at the reactor scale. Furthermore, unsteady flow structures appear everywhere in the column, as noted by Noël de Nevers in 1968 (De Nevers 1968). In this so-called heterogeneous regime, the increase of the void fraction with V_{sg} is significantly slowed down while the apparent rise velocity V_{sg}/ε steadily increases with V_{sg} and becomes much larger than U_T (Krishna, Wilkinson & Van Dierendonck 1991; Ruzicka 2013). This heterogeneous regime is exploited in many applications, but its hydrodynamics remains poorly understood. In particular, it is of practical importance to know how to scale-up bubble columns from laboratory prototypes to actual industrial plants. However, and as shown by the successive reviews, notably from Joshi *et al.* (1998), Kantarci, Borak & Ulgen (2005), Rollbusch *et al.* (2015), Kikukawa (2017) and Besagni, Inzoli & Ziegenhein (2018), there is still no consensus on appropriate scaling rules.

Recently, we have shown that, in the heterogeneous regime, buoyancy equilibrates inertia (Mezui, Obligado & Cartellier 2022) and that feature leads to velocities scaling as $(gD\varepsilon)^{1/2}$, where D is the bubble column diameter, ε the void fraction and g the gravitational acceleration. This scaling was shown to hold for mean velocities and for standard deviations. In addition, it applies to the liquid phase as well as to the gas phase. This result was found valid over a wide range of flow conditions (namely $0.1\,\mathrm{m} \leq D \leq 3\,\mathrm{m}$ and $4\text{–}5\,\mathrm{cm\,s^{-1}} \leq V_{sg} \leq 60\,\mathrm{cm\,s^{-1}}$) when considering air–water systems involving bubbles with an equivalent diameter between approximately 3 and 10 mm (Mezui *et al.* 2022). To complement that proposal, and inspired by a Zuber & Findlay approach (Zuber & Findlay 1965), the void fraction on the column axis ε_{axis} was correlated with the Froude number (defined as $Fr = V_{sg}/(gD)^{1/2}$). A direct consequence of these findings is that the relative velocity U_R, defined as the difference between the mean gas and the mean liquid vertical velocities, is also evolving as $(gD\varepsilon)^{1/2}$: the relative velocity is thus expected to increase both with the bubble column diameter and with the void fraction.

The change of the relative velocity with the void fraction is in qualitative agreement with experimentally observed trends since the apparent relative velocity either estimated as V_{sg}/ε (Krishna *et al.* 1991; Ruzicka 2013) or derived from a one-dimensional (1-D) kinematic approach (Raimundo *et al.* 2019) monotonously increases with the gas superficial velocity and, hence, with the void fraction. Furthermore, in Euler–Euler numerical simulations, the enhanced relative motion at large gas content is commonly enforced by introducing an *ad hoc* swarm coefficient (e.g. McClure *et al.* 2017; Gemello *et al.* 2018) that quantifies the decrease of the drag force acting on a bubble with the local void fraction (Ishii & Zuber 1979; Simonnet *et al.* 2007).

Concerning the impact of the bubble column diameter, there is no indisputable experimental evidence of the dependency of U_R on D. Moreover, to the best of our knowledge, the swarm coefficients introduced in simulations never depend on D. Overall, it is not physically clear why U_R should increase with the column diameter.

Hereafter, we investigate the origin of the relative velocity in the heterogeneous regime. Some preliminary results presented by Raimundo *et al.* (2019) indicate that concentration gradients should play a role in the flow dynamics. In particular, and as in turbulent convection, strong velocity differences were anticipated between zones in the flow with high void fraction and regions with low void fraction. To pursue the analysis, we need to get access to refined variables such as local concentration statistics and also to statistics on bubble velocity conditioned by the local concentration. To this end, we took the benefit of the newly developed Doppler optical probe (a technology patented by the A2 Photonic Sensors company) that simultaneously provides the gas phase indicator function and the translation velocity of bubbles (Lefebvre *et al.* 2022).

This manuscript is structured as follows. In § 2, the experimental conditions are presented and key variables such as void fraction and mean velocities characterising the bubble column behaviour are provided. In § 3, local void fraction measurements are introduced that pave the way to gather statistics on gas velocity measurements conditioned by the local gas concentration. Meso-scale structures are also presented together with their main characteristics. The term meso-scale alludes to important scales present in the flow that are between the bubble size (or the Kolmogorov scale) and the outer dimensions of the system. As it will be better detailed below, in the present work, they refer to clusters, voids and their corresponding intermediate regions. Section 4 provides conditional bubble velocity measurements for clusters, intermediate regions and void regions and the contributions of these meso-scale structures to the absolute bubble velocity and to the relative bubble velocity are discussed. In § 5, a model relating bubble conditional velocities to the size and the concentration of the corresponding meso-scale structures is proposed and successfully tested. The relevance of a $(gD\varepsilon)^{1/2}$ scaling for the relative velocity is also debated. Finally, in § 6, we show that, according to the internal flow topology, a fast-track mechanism is potentially at play that would explain why velocity fluctuations also scale as $(gD\varepsilon)^{1/2}$ in heterogeneous bubble columns.

2. Experimental conditions and unconditional velocity measurements

The experiment is the one exploited by Mezui *et al.* (2022). It consists in a 3 m high and $D = 0.4$ m internal diameter air–water bubble column. The water quality was such that coalescence was absent or at least very weak. The injector is a 10 mm thick Plexiglass plate perforated by 352 orifices (with 1 mm internal diameter) uniformly distributed over the cross-section. The static liquid height H_0 was set to 2.02 m, a value large enough to avoid any sensitivity of measurements to H_0. Experiments were performed for V_{sg} ranging from $0.6\,\mathrm{cm\,s^{-1}}$ to $26\,\mathrm{cm\,s^{-1}}$. Information relative to bubbles were acquired with a Doppler probe (Lefebvre *et al.* 2022). Such a probe ensures the detection of phases with a high resolution (its latency length is $\approx 6\,\mu$m) and it provides the velocity of bubbles. Liquid phase statistics were obtained from a Pavlov tube (see Mezui *et al.* 2022; Mezui, Cartellier & Obligado 2023 for additional details). Over the range of flow conditions considered, the mean equivalent bubble diameter remained within the interval [6.62 mm; 7.35 mm], so that the particle Reynolds number evolved in the range 1450–1550. Measurements were achieved in the quasi fully developed region at $H/D = 3.625$, where transverse profiles of velocity and void fraction are self-similar when normalised by the relevant value taken on the column axis.

To qualify the bubble column behaviour, we report in figure 1 the void fraction, and the mean bubble and liquid vertical velocities on the axis of the column versus the superficial gas velocity v_{sg}. The mean velocities correspond to statistics combining

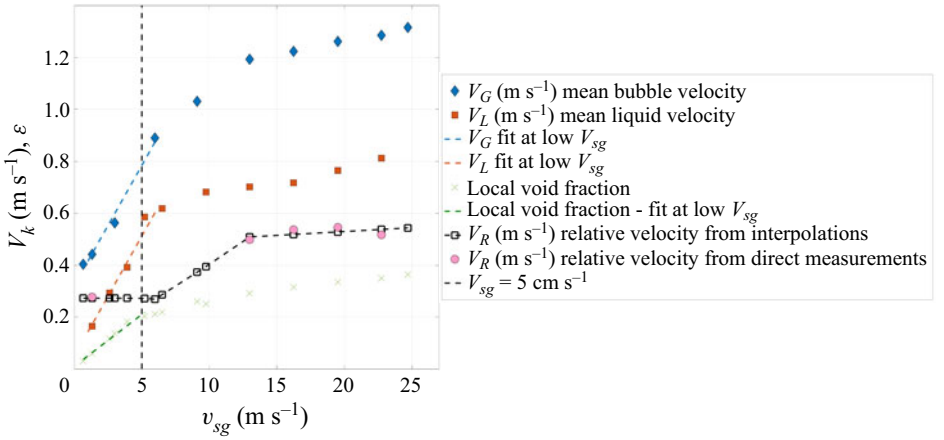

Figure 1. Evolution of the void fraction, and of mean vertical velocities of bubbles V_G and of the liquid V_L with the gas superficial velocity V_{sg}. The relative velocity has been derived from raw measurements performed at the same V_{sg} (pink dots), and from interpolations of phasic velocities versus V_{sg} (black squares). The straight lines in the homogeneous regime are linear fits of the data. Measurements performed in a $D = 0.4$ m column, at $H/D = 3.625$ and on the column axis. The vertical black dashed line indicates the transition from the homogeneous to the heterogeneous regime at $v_{sg} \sim 5\,\mathrm{cm\,s^{-1}}$.

upward and downward motions (see the discussion in Mezui *et al.* 2022). The homogeneous–heterogeneous transition is indicated by the vertical dash line at $V_{sg} = 5\,\mathrm{cm\,s^{-1}}$. Direct relative velocity measurements gathered whenever V_G and V_L data were available for the same gas superficial velocity are also plotted in figure 1 (see pink dots). We also use interpolations of U_G and V_L to estimate the relative velocity for others V_{sg} values. In particular, the linear fits of the mean bubble and liquid velocities in the homogeneous regime are parallel indicating that the relative velocity is constant in that regime. The latter amounts to $\approx 27\,\mathrm{cm\,s^{-1}}$, which is close to the terminal velocity U_T. From the transition, the relative velocity clearly increases with V_{sg}, up to $V_{sg} \approx 13\,\mathrm{cm\,s^{-1}}$. At larger V_{sg}, that is, deeper in the heterogeneous regime, the relative velocity happens to nearly stabilise at approximately 2.3–$2.5U_T$. Note, however, that in that range, and according to the few available data, the relative velocity is still smoothly increasing with V_{sg}.

Overall, figure 1 indisputably demonstrates that the relative velocity increases well beyond U_T in a bubble column operated in the heterogeneous regime. In that regime, and in terms of the scaling rule proposed by Mezui *et al.* (2022), the data gathered in the $D = 0.4$ m column correspond to $V_G \approx 1.09(gD\varepsilon)^{1/2}$ and $V_L \approx 0.67(gD\varepsilon)^{1/2}$, where ε is the local void fraction on the column axis at $H/D = 3.625$. The prefactors given here are derived from the data collected for $v_{sg} \geq 13\,\mathrm{cm\,s^{-1}}$, but, as shown in Mezui *et al.* (2022), they hold over a significant range of column diameters and of flow conditions. Hence, the relative velocity in the heterogeneous regime and far enough from the transition is expected to behave as

$$U_R \approx 0.41(gD\varepsilon)^{1/2}. \tag{2.1}$$

Equation (2.1) predicts that the relative velocity depends on the column diameter, a feature that is not trivial. To understand the origin of the relative velocity in these buoyancy-driven bubbly flows, we focus our analysis on the connection between local concentration and bubble velocity. In the next section, a local void fraction is defined and related statistics are discussed.

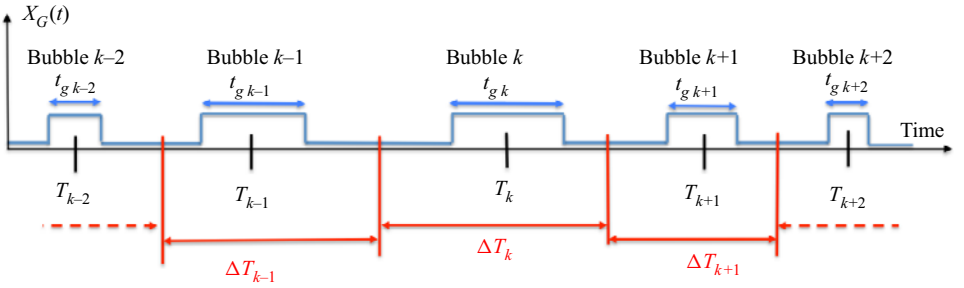

Figure 2. Construction of a 1-D Voronoï tessellation from the gas phase indicator function.

3. Local void fraction and meso-scale structures

3.1. *Local void fraction and identification of meso-scale structures*

Paralleling what we did for turbulent particle-laden flows (Monchaux, Bourgoin & Cartellier 2010; Sumbekova *et al.* 2017; Mora *et al.* 2018), we exploit 1-D Voronoï tessellations built from the gas phase indicator function $X_G(t)$ (Raimundo 2015; Mezui, Cartellier & Obligado 2018; Raimundo *et al.* 2019). Here, $X_G(t)$ is deduced from the signal delivered by an optical probe. For the gas phase indicator function measurements presented here, the probe orientation was held fixed (the probe was directed downwards). As shown in figure 2, Voronoï cells are then built as successive time intervals, each containing a single bubble. For that, the centres T_k of successive gas residence times t_{gk} are identified. The mid-distance between successive centres T_k and T_{k+1} defines a Voronoï cell boundary. This process is repeated for all detected bubbles, and the width of the kth Voronoï cell that contains the kth bubble is given by $\Delta T_k = (T_{k+1} - T_{k-1})/2$.

Probability density functions (p.d.f.s) of the Voronoï cell width ΔT_k normalised by the average $\langle \Delta T_k \rangle$ are presented in figure 3(a) for various gas superficial velocities: all these data have been collected on the bubble column axis at $H/D = 3.625$. Care was taken to ensure a correct convergence of these distributions. The latter comprises between 8000 and 13 000 bubbles: these samples correspond to measuring durations from 95 to 950 s depending on flow conditions.

Qualitatively, the width ΔT_k of the time interval containing the kth bubble is an indication of the local concentration. A short duration ΔT_k means the presence of a close-by bubble while a large duration indicates that the kth bubble is somewhat isolated. We will come back later to the connection between normalised cell durations $\Delta T_k/\langle \Delta T_k \rangle$ and concentration. For the time being, let us focus on the allure of these p.d.f.s. The dash line in figure 3(a) represents the p.d.f. of normalised cell durations $\Delta T_k/\langle \Delta T_k \rangle$ for a random Poisson process – RPP in short (Ferenc & Néda 2007) – that has no correlation at any scale. Clearly, and as noted by Raimundo *et al.* (2019), measured distributions at large enough V_{sg} differ from the RPP case. In particular, both very large cell durations (corresponding to dilute conditions) and very small cell durations (corresponding to dense conditions) are more probable than for an RPP. Figure 3(c,d) show the p.d.f. with non-normalised cell durations (ΔT_k) and with the alternative normalisation $\Delta T_k/(D/V_{sg})$, respectively. The latter represents a large-scale time scale for the gas phase, and gives similar results in the heterogeneous regime than the normalisation $\Delta T_k/\langle \Delta T_k \rangle$.

Following Monchaux *et al.* (2010), the distance to an RPP is commonly appreciated by examining the standard deviation $\sigma_{voronoi}$ of the p.d.f. of Voronoï cells widths. As shown in figure 3(b), such standard deviation drastically increases from a low value, comparable

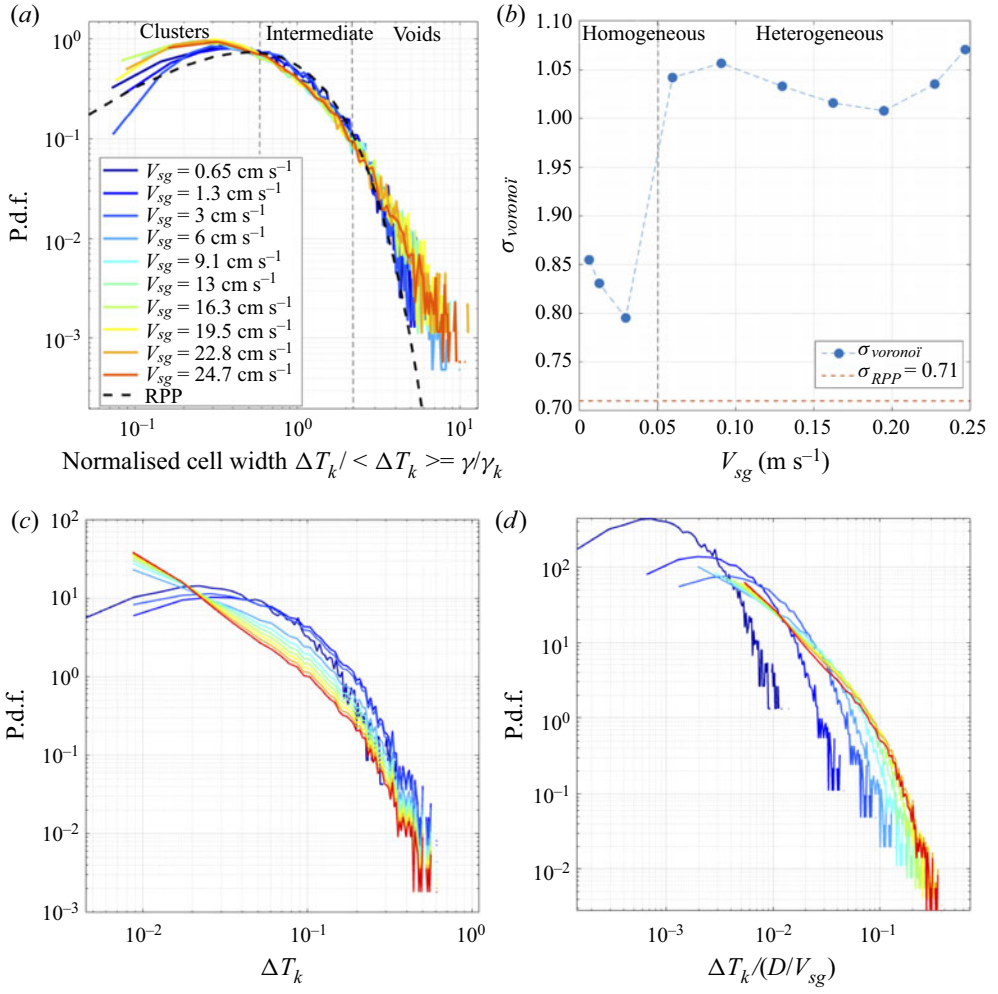

Figure 3. (*a*) Centred p.d.f.s of 1-D Voronoï cells width $\Delta T_k/\langle \Delta T_k \rangle$ built from Doppler probe signals at various gas superficial velocities. The dash line represents the 1-D Voronoï distribution for an RPP, i.e. a random Poisson process. The vertical dashed lines indicate the thresholds for the definitions of clusters and voids (as defined by Monchaux *et al.* 2010). (*b*) Evolution of the standard deviation of 1-D Voronoï distributions with the gas superficial velocity. The horizontal dash line indicates the standard deviation for an RPP while the vertical dashed line delineate the homogeneous–heterogeneous transition. Measurements performed in a $D = 0.4$ m column, on the column axis at $H/D = 3.625$. P.d.f.s of 1-D Voronoï cells width (*c*) ΔT_k and (*d*) $\Delta T_k/(D/V_{sg})$. We remark that in the last two panels the binning used to compute the p.d.f.s calculation is different from panel (*a*).

to that of an RPP, to a much higher value (close to unity) when the system shifts from the homogeneous to the heterogeneous regime. In the homogeneous regime, the measured standard deviation of Voronoï cells p.d.f.s evolves between 0.8 and 0.85. This is slightly larger than the 0.71 limit for an RPP of point particles as determined by Ferenc & Néda (2007) (according to Uhlmann (2020), the standard deviation for an RPP with finite-size particles is even lower). The origin of that small difference is unclear. This could be the mark of an inhomogeneous spatial repartition of bubbles in the homogeneous regime because of some gas maldistribution at injection (Nedeltchev 2020): such a scenario is

supported by the analysis of liquid velocity profiles (Lefebvre *et al.* 2022). Alternately, that small difference could be due to the measuring method itself because the optical probe allows detecting the centres of gas chords and not the centres of bubbles, and because most bubbles are not spherical. Hence, the value of the standard deviation measured in the homogeneous regime could be interpreted at the reference RPP level as detected with the probe technique. The key points in figure 3(*b*) are the very sharp increase in $\sigma_{voronoi}$ observed at the homogeneous–heterogeneous transition, and the large value, well above that of an RPP, that $\sigma_{voronoi}$ reaches at high V_{sg}. The shortcomings of 1-D Voronoï analysis in complex flows have been discussed elsewhere (Mora *et al.* 2018, 2019): one key result is that the clear difference observed with the standard deviation of an RPP unambiguously demonstrates that clustering does occur in the present flow conditions. Furthermore, for all heterogeneous conditions investigated (that is, for V_{sg} up to $24\,\mathrm{cm\,s^{-1}}$), the standard deviation $\sigma_{voronoi}$ remains nearly the same: that feature also indicates that clustering is a central characteristic of the heterogeneous regime. Finally, let us underline that, as for turbulent flows laden with inert particles (Sumbekova *et al.* 2017), the main contribution to the standard deviation comes from cells at large $\Delta T_k/\langle\Delta T_k\rangle$ corresponding to low void fractions, compared with the contribution from cells with intermediate $\Delta T_k/\langle\Delta T_k\rangle$ (void fractions close to the mean value) or with low $\Delta T_k/\langle\Delta T_k\rangle$ (high void fractions).

To quantify the connection between cell width $\Delta T_k/\langle\Delta T_k\rangle$ and concentration, we consider two approaches. First, we follow what we did for a turbulent flow laden with droplets (Sumbekova *et al.* 2017; Mora *et al.* 2018), by connecting the ratio $\Delta T_k/\langle\Delta T_k\rangle$ to linear number densities, i.e. with the number of inclusions detected per unit length. The length corresponds to the measuring duration multiplied by the axial velocity V_{axial} of inclusions. The local number density γ_k (number of inclusions per meter) in the kth cell equals $1/[\Delta T_k V_{axial}]$, while $1/[\langle\Delta T_k\rangle V_{axial}]$ is the mean number density γ. Therefore, the normalised cell width $\Delta T_k/\langle\Delta T_k\rangle = \gamma/\gamma_k$ represents the inverse of the instantaneous (i.e. at the scale of the Voronoï cell) number density divided by the mean number density. When applied to bubble columns (Raimundo 2015; Mezui *et al.* 2018; Raimundo *et al.* 2019), we considered V_{axial} as the mean bubble velocity, and γ was assumed to be proportional to the mean dispersed phase concentration. Under these assumptions, the inverse of $\Delta T_k/\langle\Delta T_k\rangle$, i.e. γ_k/γ, provides the magnitude of the local gas concentration (local at the scale of the Voronoï cell) with respect to the mean gas fraction at the measuring location. In figure 3(*a*), the abscissa $\Delta T_k/\langle\Delta T_k\rangle$ varies from 0.07 to 10 so that γ_k/γ covers more than two decades as it evolves between 0.1 and approximately 14.

However, a second approach is required because, for the heterogeneous conditions considered here, γ_k/γ does not coincide with the ratio $\varepsilon_k/\varepsilon$ of the void fraction ε_k relative to the kth cell to the mean gas hold-up ε at the measuring location. Indeed, in the turbulent particle-laden flows we have previously analysed, all inclusions travelled with almost the same axial velocity. This is no longer the case for bubbles in the heterogeneous regime as their velocities experience strong variations (see figure 2 in Mezui *et al.* 2022), leading to a standard deviation as large as 60 % of the mean. Hence, the selection of a mean bubble velocity to transform time into space induces very large distortions on the concentration estimate by way of γ_k. To correct for these distortions and to evaluate reliable local void fractions, it is appropriate to rely on gas residence times as the latter naturally account for the actual velocity of each bubble. The void fraction relative to the kth Voronoï cell equals the sum of gas residence times included in that cell divided by the cell duration ΔT_k. As shown in Appendix A, the ratio $\Delta T_k/\langle\Delta T_k\rangle$ is indeed related to $\varepsilon/\varepsilon_k$, but it does not coincide with $\varepsilon/\varepsilon_k$ as the prefactor between these two quantities varies with the gas residence time (see (A1) in Appendix A). In consequence, in the following, we will use

	Dense regions	Intermediate regions	Empty regions
Repartition of bubbles in number in measured p.d.f.s in the heterogeneous regime (average values for $V_{sg} \geq 9\,\mathrm{cm\,s^{-1}}$)	38 %	57 %	5 %
Repartition of the actual void fraction $\varepsilon_k/\varepsilon$ in the heterogeneous regime (average for $V_{sg} \geq 9\,\mathrm{cm\,s^{-1}}$)	17 %	73 %	10 %
Repartition of bubbles in number in RPP	30 %	68 %	2 %
Repartition of the actual void fraction $\varepsilon_k/\varepsilon$ in the homogeneous regime (average values for $V_{sg} \leq 3\,\mathrm{cm\,s^{-1}}$)	29 %	67 %	4 %
Repartition of bubbles in number in measured p.d.f.s in the homogeneous regime (values for $V_{sg} = 1.3\,\mathrm{cm\,s^{-1}}$)	33.60 %	63.20 %	3.20 %

Table 1. Typical distributions of the dispersed phase between void regions, intermediate regions and dense regions in the heterogeneous and homogeneous regimes and comparison with an RPP. From measurements on the axis of a $D = 0.4$ m bubble column at $H/D = 3.625$.

the ratio γ_k/γ as a crude, qualitative characterisation of meso-scale structures in terms of concentration, while exact measurements of the gas fraction $\varepsilon_k/\varepsilon$ will be considered in § 5 for discussing modelling issues.

Going back to figure 3(*a*), and whatever the flow conditions, the measured p.d.f.s of Voronoï cells cross the RPP at two fixed abscissa represented by vertical dashed lines. A third intersection sometimes occurs in the very dense limit (at $\Delta T_k/\langle \Delta T_k \rangle$ approximately 0.1, that is, for γ_k/γ approximately 10), but it will not be considered here because its occurrence is far too sensitive to the sample size. As for turbulent particle-laden flows (Monchaux *et al.* 2010), we define three populations out of the two stable thresholds. A Voronoï cell (and the bubble it contains) belongs to a 'dense' region when $\Delta T_k/\langle \Delta T_k \rangle$ is below 0.51, or equivalently when γ_k/γ is higher than 1.96. A Voronoï cell (and the bubble it contains) belongs to an 'empty' or 'void' region when $\Delta T_k/\langle \Delta T_k \rangle$ is above 2.89, or equivalently when γ_k/γ is lower than 0.34. In between, the cell (and its bubble) pertains to an 'intermediate' region. Let us underline that these thresholds are stable with respect to V_{sg} (see figure 3*a*). They seem also independent of the column diameter as the same thresholds were observed for a $D = 1$ m column at $V_{sg} = 0.25\,\mathrm{m\,s^{-1}}$ (see figure 11 in Raimundo *et al.* 2019).

Owing to figure 3(*a*), the probability for bubbles to belong to 'empty' or to 'dense' regions is larger than in RPP. This is confirmed by the data presented in table 1. On average, 38 % of the bubbles belong to dense regions, while 5 % are within empty regions and 57 % are in intermediate regions: these figures remain stable within approximately 5 % over the whole heterogeneous regime, that is, for V_{sg} from $6\,\mathrm{cm\,s^{-1}}$ to $25\,\mathrm{cm\,s^{-1}}$. As expected, the figures relative to dense and to empty regions are significantly larger than those for an RPP. Table 1 also confirms that, in the homogeneous regime, the repartition of bubbles in number between dense, empty and intermediate regions is very close to the repartition in number for an RPP.

The difference between homogeneous and heterogeneous conditions is also manifest in terms of void fractions. In the heterogeneous regime, the contributions to the local void fraction are typically 17 % for the dense regions, 10 % for the empty regions and 70 % for intermediate regions (table 1). These values correspond to average values for

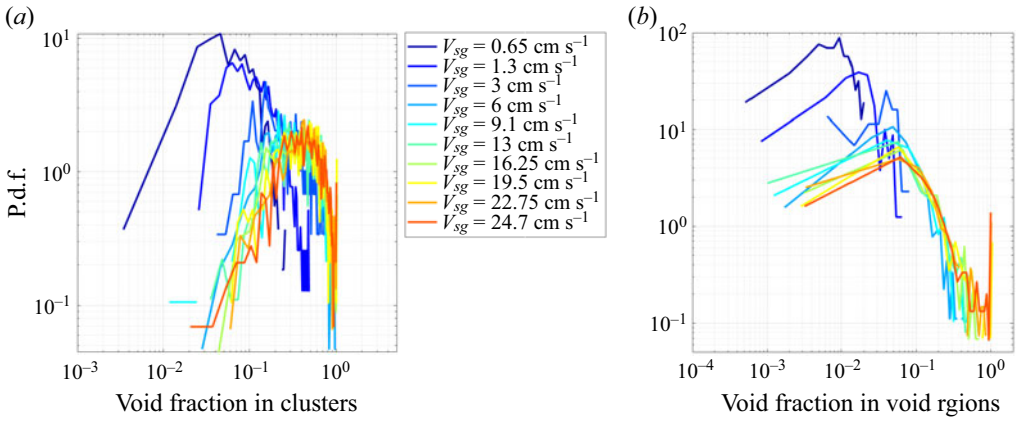

Figure 4. P.d.f.s of void fraction (in absolute value) (*a*) in clusters and (*b*) in void regions for different superficial velocities. For these statistics, we considered clusters comprising at least two bubbles. Measurements performed in a $D = 0.4$ m column, on the column axis at $H/D = 3.625$.

$V_{sg} \geq 9\,\mathrm{cm\,s^{-1}}$: they change by less than 1 % when considering data over the interval $V_{sg} \geq 6\,\mathrm{cm\,s^{-1}}$. Note that there is a slight decrease of the contribution of dense regions to the local void fraction as V_{sg} increases, which is compensated by a slight increase with V_{sg} of the contributions of empty and intermediate regions.

3.2. *Characterisation of meso-scale structures*

Once all bubbles have been distributed within the three populations, meso-scale structures are then formed using the following procedure. Bubbles belonging to a 'dense' region and successive in time are assembled to form a 'cluster'. Similarly, successive bubbles belonging to an 'empty' region are assembled to form a 'void'. The same process was used for intermediate regions. The characteristics of the resulting meso-scale structures in terms of size and concentration are then extracted.

(i) The void fraction (in absolute value) in a given meso-scale structure is evaluated as the sum of gas residence times for all bubbles pertaining to that structure divided by the duration of that structure, the later being the sum of all involved ΔT_k. The distributions of void fraction in clusters and in voids are exemplified in figure 4 for various V_{sg}.

(ii) The size of a given meso-scale structure is estimated as the duration of the structure multiplied by the average bubble velocity, the latter being evaluated for the bubbles belonging to the structure considered: these conditional velocities are analysed in the next section. Length distributions for clusters and for voids are provided in figure 5 for various V_{sg}.

We considered two options for clusters: either the minimum number of bubbles in a cluster is set to one so that all Voronoï cells with a $\Delta T_k/\langle \Delta T_k \rangle$ below the threshold are considered as clusters, or the minimum number of bubbles is set to two so that clusters involving a single bubble are excluded. The second option has been suggested to help distinguishing between 'coherent' and 'random' clusters in turbulent particle-laden flows (Mora *et al.* 2019). Here, and for all the flow conditions pertaining to the heterogeneous regime, it happens that 37 % to 40 % of clusters involve a single inclusion.

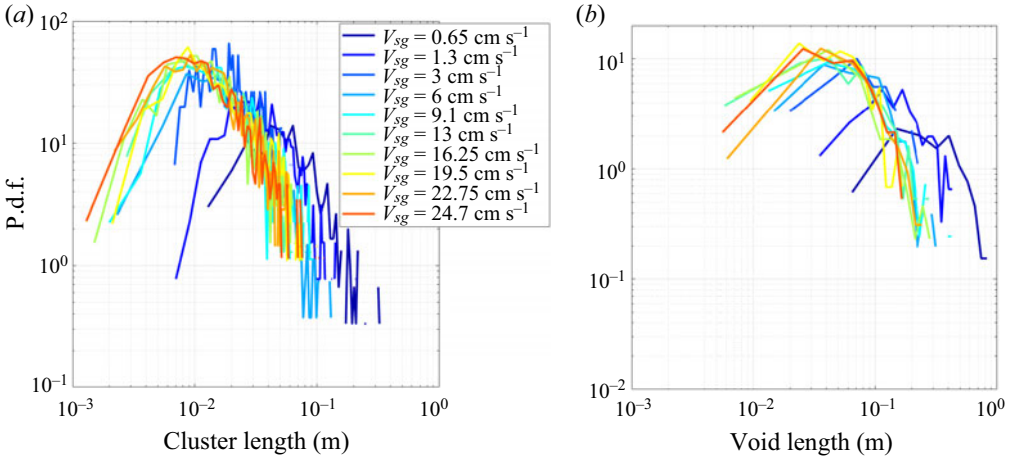

Figure 5. P.d.f.s of lengths (*a*) of clusters and (*b*) of void regions for different superficial velocities. For these statistics, we considered clusters that comprise at least two bubbles. Measurements performed in a $D = 0.4$ m column, on the column axis at $H/D = 3.625$.

It should also be underlined that zones below or beyond the above-defined thresholds also exist for an RPP. Hence, one can still identify and statistically characterise 'dilute' and 'dense' regions in homogeneous conditions even though the corresponding Voronoï distributions are very close to and/or almost collapse with an RPP. Using the same data processing routine to analyse homogeneous and heterogeneous conditions, the characteristics of clusters and of empty regions are presented over the whole range of V_{sg} from homogeneous to heterogeneous regimes, bearing in mind that different physical origins are associated with meso-scale structures for these two regimes. In particular, the data in the homogeneous regime are not expected to bear any particular significance as they could be of random origin, or they could be related to some correlation induced by 'defects' in the system (due for example to gas injection, see Lefebvre *et al.* 2022).

Figures 4 and 5 clearly demonstrate that, for void regions as well as for clusters, the distributions in the heterogeneous regime markedly differ from the distributions observed in the homogeneous regime. Moreover, in the heterogeneous regime, the distributions tend to collapse indicating that clusters and void regions reach an asymptotic state when the gas superficial velocity becomes large enough. As shown in figure 6, that limiting state is almost the same when considering clusters with a minimum of one bubble or with a minimum of two bubbles.

The average characteristics of clusters and of void and intermediate regions are given in figure 7 as a function of the gas superficial velocity.

(i) The average number of bubbles is approximately 1.8 in void regions and approximately 4 in intermediate regions. In clusters, it is approximately 4.5 when $n \geq 2$, and it drops to 3.2 when accounting for clusters consisting of a single bubble. The decrease from 4.5 to 3.2 is consistent with the fact that, as seen above, 2/3 of the clusters comprise more than one bubble. These average numbers of bubbles are quite low: they indicate that the clusters are not organised as compact assemblies of bubbles, but are more like thin sheets. The fact that the probability to find a cluster comprising N bubbles decays like $N^{-1.17}$, i.e. that it strongly drops with N, also supports the proposed picture. In particular, 1-D clusters comprising more than ten bubbles are very rare: they represent only 3.7 % of the clusters (with $n \geq 1$) present in the heterogeneous regime.

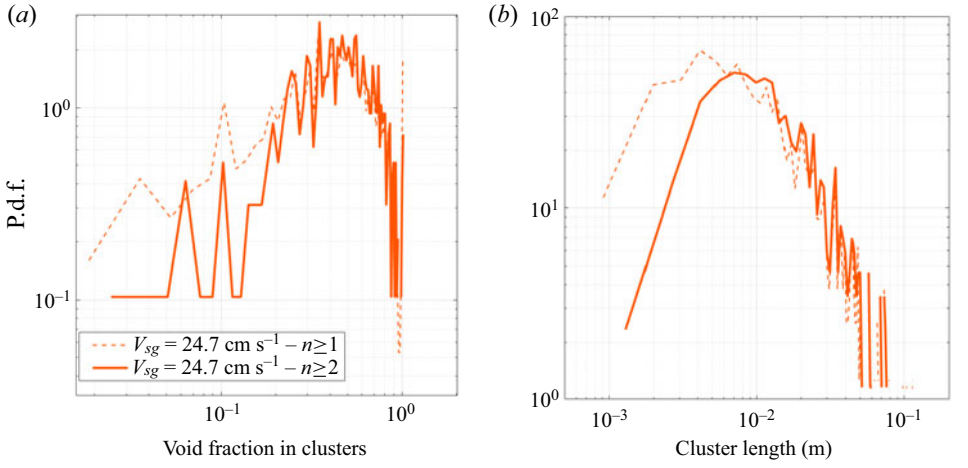

Figure 6. Comparisons of the p.d.f.s (*a*) of void fraction in clusters and (*b*) of cluster lengths when the minimum number of bubbles is set to one or to two. Measurements performed in a $D = 0.4$ m column, on the column axis at $H/D = 3.625$ and $V_{sg} = 24.7\,\mathrm{cm\,s^{-1}}$.

(ii) The size of void regions and of intermediate regions varies from 6–7 cm to 20 cm while the size of clusters ranges from a few millimetres up to 6–7 cm. In the heterogeneous regime, the mean size of clusters $\langle L_{cluster}\rangle$, that of void regions $\langle L_{void}\rangle$ and that of intermediate regions $\langle L_{int}\rangle$ all remain fairly stable. The mean cluster length asymptotes at 21 ± 3 mm: it is marginally affected if one considers a minimum of one bubble instead of two to form clusters. The asymptotic mean length of void regions is significantly larger as $\langle L_{void}\rangle\rangle \sim 74\,\mathrm{mm} \pm 10\,\mathrm{mm}$, and similarly, for intermediate regions, $\langle L_{int}\rangle$ is approximately $62\,\mathrm{mm} \pm 4\,\mathrm{mm}$.

(iii) The average concentration (in absolute value) in voids steadily increases with the gas superficial velocity. A similar behaviour holds for intermediate regions. In clusters, the average concentration sharply increases at the homogeneous–heterogeneous transition, and for V_{sg} above $\sim 0.15\,\mathrm{m\,s^{-1}}$, it tends to stabilise at a large void fraction, say approximately 50 %. Interestingly, when scaled by the local void fraction ε (here ε equals the void fraction on the axis ε_{axis}), the mean concentrations in voids and in intermediate regions increase with the mean gas hold-up, while the concentration in clusters slightly decreases: additional data are needed to confirm if the asymptotic trend corresponds to a decrease or to a plateau. The same question holds concerning the asymptotic behaviour of the difference in concentration between dense and dilute regions.

4. Absolute and relative bubble velocities conditioned by the local concentration

Paralleling what we did for turbulent particle-laden flows (Sumbekova *et al.* 2016), bubbles are classified into three populations namely clusters, void regions and intermediate regions. Bubble velocity p.d.f.s are built for each of these populations using direct velocity measurements (no interpolation) performed with a downward oriented Doppler probe (Lefebvre *et al.* 2022). Examples of such conditional p.d.f.s are provided figure 8. For both regimes, the minimum velocities are approximately the same for the three populations, while the most probable velocity as well as the maximum velocity drift to larger values when successively considering void regions, intermediate regions and clusters. This drift is weak in the homogeneous regime: the velocity at the peak increases from approximately

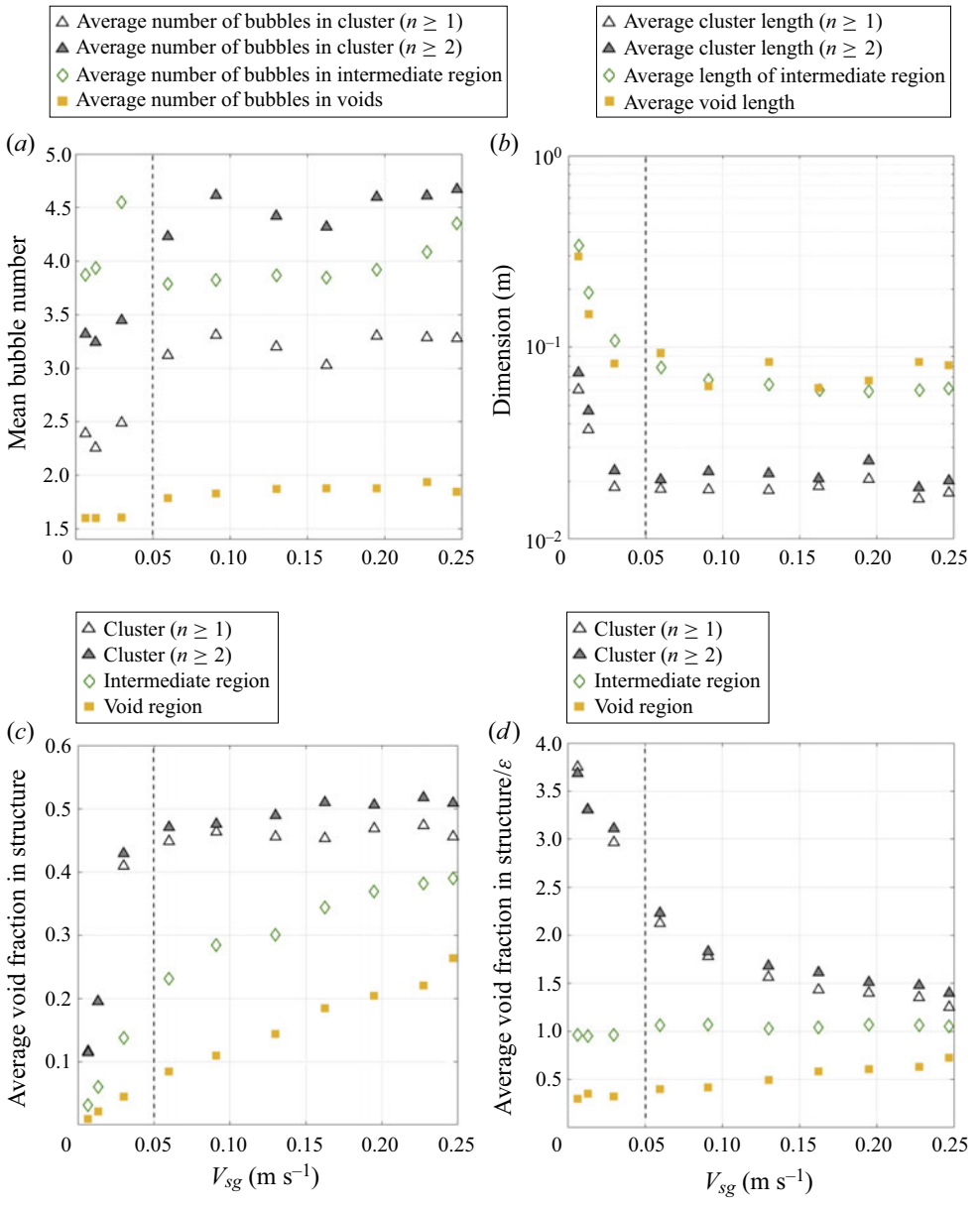

Figure 7. Mean characteristics of clusters, of void regions and of intermediate regions versus the gas superficial velocity: (*a*) average number of bubbles in meso-scale structures; (*b*) average size; (*c*) average absolute gas concentration in meso-scale structures; (*d*) average concentration scaled by the void fraction on the column axis. Measurements performed in a $D = 0.4$ m column, on the column axis, at $H/D = 3.625$. Vertical dashed lines delineate the homogeneous to heterogeneous transition.

0.4 m s^{-1} in void regions to 0.7 m s^{-1} in clusters, so that the difference is of the order of the bubble terminal velocity. The drift is significantly larger in the heterogeneous regime as the most probable velocity goes from ∼0.5 m s^{-1} in void regions up to 1.3 m s^{-1} in clusters: in that case, the difference amounts to 3.5 times the bubble terminal velocity. Hence, the conditional bubble velocities gathered with the Doppler optical probe confirm

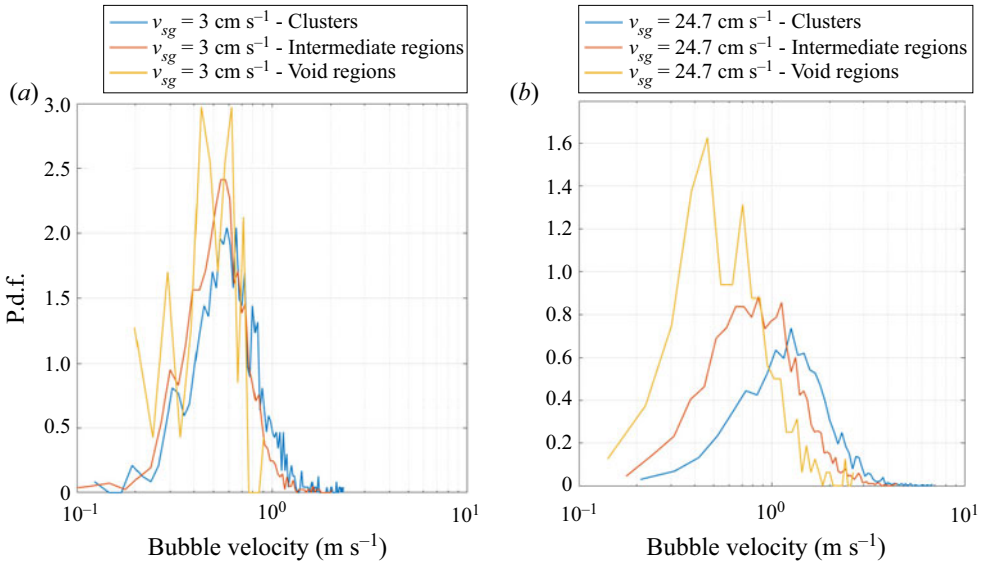

Figure 8. Bubble velocity p.d.f.s conditioned by the meso-scale structure they belong to, i.e. clusters, intermediate regions or void regions (*a*) for $V_{sg} = 3\,\mathrm{cm\,s^{-1}}$ and (*b*) for $V_{sg} = 24.7\,\mathrm{cm\,s^{-1}}$. Measurements performed in a $D = 0.4$ m column, on the column axis at $H/D = 3.625$ with a downward directed Doppler probe.

our physical expectation that, on average, high void fraction regions are moving up much faster than low void fraction regions.

To quantify this effect, and for each meso-scale structure, we evaluated the mean bubble velocity $V_{b|s}$ for bubbles pertaining to the selected meso-scale structure. These velocities, which represent absolute velocities in the laboratory frame, are shown in figure 9 as a function of the gas superficial velocity. It could be observed that the average conditional velocities relative to void regions $V_{b|voids}$, to intermediate regions $V_{b|int}$ and to clusters $V_{b|cluster}$, all monotonously increase with V_{sg}. In addition, the velocity differences between any two out of these three populations remain limited, of the order of U_T, in the homogeneous regime. Beyond the homogeneous–heterogeneous transition, the velocity differences clearly increase with V_{sg}: bubbles embedded in dense regions are moving up faster than bubbles in intermediate regions, which are themselves moving up faster than bubbles in dilute regions. This observation provides indisputable evidence of the central role of meso-scale structures on the actual dynamics of bubbles in the heterogeneous regime.

In figure 9, we have reported the unconditional mean vertical bubble velocity V_G shown in figure 1 (green dots). In the heterogeneous regime, V_G happens to be comprised between $V_{b|int}$ and $V_{b|cluster}$. It is tempting to try to recover the unconditional bubble velocity V_G from conditional measurements. Considering that a fraction $N_{cluster}$ of bubbles pertains to clusters, that a fraction N_{int} belongs to intermediate regions and a fraction N_{void} to void regions (with $N_{cluster} + N_{int} + N_{void} = 1$), one expects that

$$V_G = N_{cluster} V_{b|cluster} + N_{int} V_{b|int} + N_{void} V_{b|void}. \tag{4.1}$$

For the heterogeneous regime, the conditional mean bubble velocities $V_{b|cluster}$, $V_{b|int}$ and $V_{b|void}$ are provided in table 2 for all the gas superficial velocities considered in the experiments. As the repartition of bubbles between the three populations is already

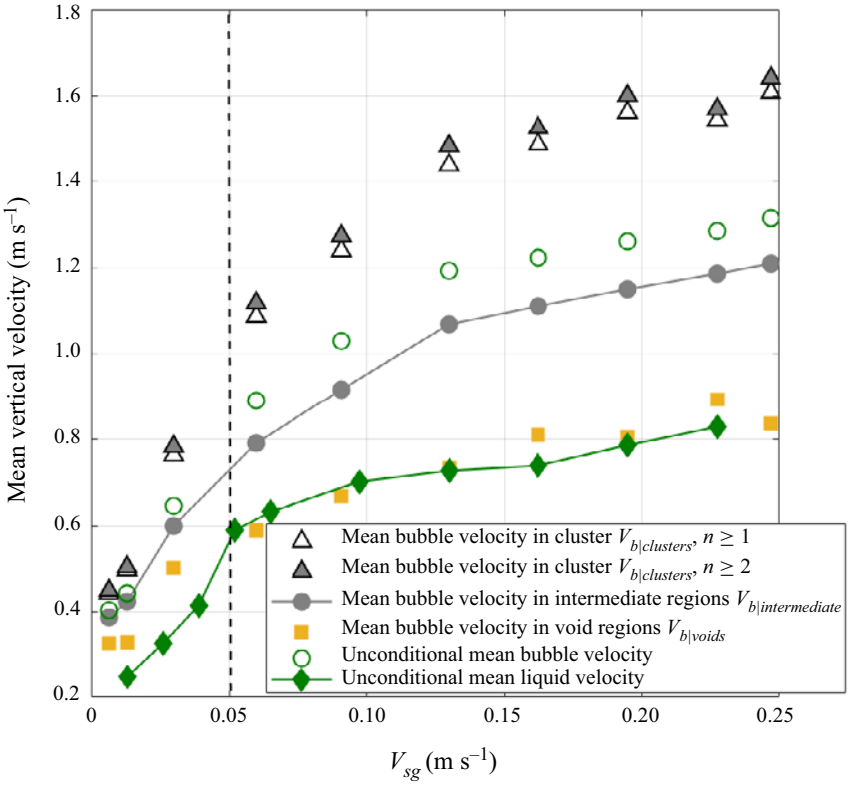

Figure 9. Average absolute bubble velocity for bubbles pertaining to clusters $V_{b|clusters}$, to intermediate regions $V_{b|int}$ and to void regions $V_{b|voids}$ versus the gas superficial velocity. Measurements performed in a $D = 0.4$ m column on the column axis at $H/D = 3.625$ with a downward directed Doppler probe. The unconditional mean liquid V_L and gas V_G velocities from figure 1 are also shown for sake of comparison.

known (see table 1), the mean bubble velocity deduced from (4.1) can be evaluated. As shown in table 2, there is an excellent agreement between the bubble velocity predicted using (4.1) and direct, unconditional measurements of the bubble velocity. Moreover, the contribution of bubbles inside clusters to their vertical transport velocity amounts to 46 %, the contribution of intermediate regions is 51 % and the remaining 3 % arise from void regions. These figures remain the same within $\pm 0.5\%$ for all V_{sg} considered in the heterogeneous regime.

These results provide more evidence that meso-scale structures have a key role in the dynamics of bubbles and notably on their absolute velocity in the heterogeneous regime. In some way, they confirm the intuition of Noel De Nevers concerning the role of internal structures, as this author argued in 1968: '*In unbaffled systems these (bubble driven) circulations are unstable and chaotically change in size, shape, and orientation. These chaotic circulations provide the principal mode of vertical bubble transport in bubble columns over a wide range of operating conditions*' (De Nevers 1968).

The same analysis was also done for the homogeneous regime. For each of the four gas superficial velocities V_{sg} considered in that regime, table 3 provides the conditional bubble velocities, the resulting unconditional bubble velocity predicted using (4.1) and the unconditional bubble velocity that was directly measured. The agreement is very good, except for a 15 % difference for one condition. Note that very similar figures would be obtained if one considers the repartition for an RPP instead of the repartition of bubbles

https://doi.org/10.1017/jfm.2023.259 Published online by Cambridge University Press

	Conditional mean bubble velocities ($m\,s^{-1}$)			Unconditional mean bubble velocities ($m\,s^{-1}$)		
V_{sg} ($m\,s^{-1}$)	Bubbles in clusters	Bubbles in intermediate regions	Bubbles in void regions	Deduced from (4.1)	Measured	difference %
0.091	1.239	0.917	0.667	1.027	1.03	−0.4
0.13	1.437	1.069	0.734	1.192	1.193	0
0.1625	1.486	1.111	0.812	1.238	1.223	1.3
0.195	1.561	1.15	0.805	1.289	1.2613	2.2
0.2275	1.544	1.186	0.894	1.307	1.285	1.8
0.247	1.609	1.21	0.836	1.343	1.3155	2
Repartition of bubbles in number (as measured)	38 %	57 %	5 %	—	—	—

Table 2. Estimations of the unconditional mean bubble velocity V_G deduced from mean bubble velocities conditioned by meso-scale structures using (4.1) in the heterogeneous regime.

https://doi.org/10.1017/jfm.2023.259 Published online by Cambridge University Press

	Conditional mean bubble velocities ($m\,s^{-1}$)			Unconditional mean bubble velocities ($m\,s^{-1}$)		
V_{sg} ($m\,s^{-1}$)	Bubbles in clusters	Bubbles in intermediate regions	Bubbles in void regions	Deduced from (4.1)	Measured	difference %
0.0065	0.442	0.387	0.327	0.404	0.404	0.04
0.013	0.497	0.424	0.329	0.446	0.442	0.6
0.0299	0.763	0.600	0.503	0.652	0.563	14.5
0.0598	1.087	0.791	0.590	0.884	0.891	−0.8
Repartition of bubbles in number (as measured)	33.6 %	63.2 %	3.2 %	—	—	—

Table 3. Estimates of the unconditional mean bubble velocity V_G deduced from mean bubble velocities conditioned by meso-scale structures using (4.1) in the homogeneous regime.

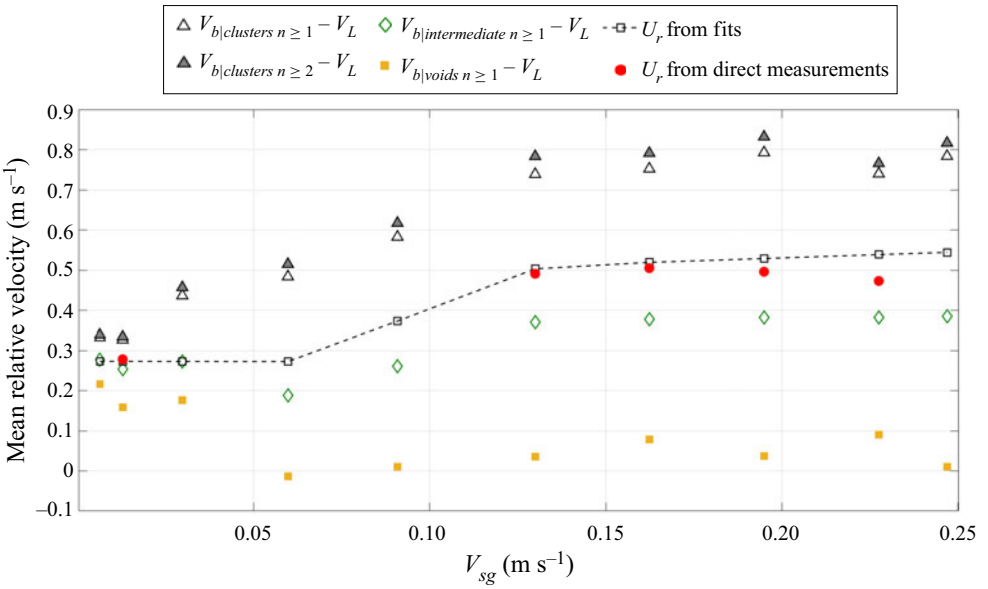

Figure 10. Mean relative velocity between bubbles pertaining to a meso-scale structure, namely clusters, intermediate regions and void regions, and the liquid phase: evolution with V_{sg}. The unconditional relative velocity U_R is also shown for comparison (red dots correspond to direct measurements while the dash line corresponds to interpolated data shown in figure 1). Measurements performed in a $D = 0.4$ m column, on the column axis at $H/D = 3.625$.

that was measured in the homogeneous regime (table 1). Therefore, (4.1) allows to recover the unconditional bubble velocity from conditional data in the homogeneous regime. However, the contributions of each population to the vertical transport velocity of bubbles are different from those found in the heterogeneous regime: they amount to approximately 39 % for clusters, 59 % for intermediate regions and 2 % for void regions.

To appreciate the role of meso-scale structures on the relative motion, we plot in figure 10 the mean bubble relative velocities with respect to the liquid phase for each meso-scale structure. As shown in figures 9 and 10 , the mean, unconditional liquid velocity is very close to the mean bubble velocity on void regions so that $V_{b|void} - V_L$ remains close to zero in the heterogeneous regime. This is not too surprising because void regions contain fewer bubbles, and also because of the bubble response time compared with its transit time through the column (see the discussion in § 6). The two velocity differences $V_{b|clusters} - V_L$ and $V_{b|int} - V_L$ increase with V_{sg} in a way similar to the unconditional relative velocity $U_R = V_G - V_L$. In particular, the differences in velocities remain moderate in the homogeneous regime, and they steeply increase at the transition. Both differences $V_{b|clusters} - V_L$ and $V_{b|int} - V_L$ tend to become more or less constant at large V_{sg} (roughly above $V_{sg} \approx 13$–15 cm s^{-1}). In intermediate regions, the average bubble velocity exceeds that of the liquid by 0.3–0.4 m s^{-1}. In clusters, the difference reaches approximately 0.7–0.8 m s^{-1}, that is, 3 to 3.5 times the bubble terminal velocity.

A decomposition similar to (4.1) can be applied to the mean bubble relative velocity, namely:

$$U_R = V_G - V_L = N_{clusters}(V_{b|clusters} - V_L) + N_{int}(V_{b|int} - V_L) + N_{voids}(V_{b|voids} - V_L). \tag{4.2}$$

Even though (4.2) can be directly deduced from (4.1), it is important to analyse the contributions of the three populations to the mean relative velocity. First, and as expected, the agreement between the measured unconditional mean bubble relative velocity as evaluated from (4.2) and as directly measured happens to be as good as that on V_G. In the homogeneous regime, the respective contributions of the three populations to the mean relative velocity remain the same as for the mean bubble velocity. In the heterogeneous regime, these proportions are changed with 57 % coming from clusters, 42 % arising from intermediate regions and less than 1 % for voids. The contribution of clusters to the relative velocity is thus significantly enhanced (with an increase by more than 10 %) compared with their contribution to the mean bubble velocity.

The fact that, for both regimes, the unconditional bubble velocity is well recovered from bubble velocities conditioned by the three meso-scale structures that were identified indicates that the data processing is reliable and robust. The important point for the dynamics lies in the respective contributions of the three populations. Let us first underline that the results presented above are provided for clusters containing at least one bubble. For both regimes, the figures remain very close when considering a minimum of two bubbles in clusters, so that our analysis is not sensitive to the precise cluster definition. Also, and as already said, the decomposition into meso-scale structures in the homogeneous regime may appear as somewhat artificial, but, owing to their definition, such structures can indeed be identified from an RPP even though their probability of occurrence is low. We also recall that the definition of frontiers between populations derives from the specific shape of the Voronoï cell p.d.f. in the heterogeneous regime. These beginnings being established, the key point here is that the velocities conditioned by structures happen to be quite different in the two regimes. In particular, the contribution of clusters to both absolute velocities and relative velocities of bubbles is significantly larger in the heterogeneous regime than in the homogeneous regime. These features are clear indications that the physics at play are different, with collective effects present in the heterogeneous regime while the repartition of bubbles and their dynamics remain quasi uniform in the homogeneous regime.

The role of meso-scale structures on the bubble motion being clarified, it would be worthwhile to develop a prediction of the velocity of bubbles pertaining to each population. This is the objective of the next section.

5. Scaling of conditional relative velocities and meso-scale structure dynamics

In Mezui *et al.* (2022), we considered an inertia-buoyancy equilibrium at the scale of the bubble column from which we derived the scaling of transport velocities for liquid and gas phases. An equilibrium involving inertia and buoyancy is now assumed at the scale of each meso-scale structure immersed in the two-phase mixture to evaluate the velocity of that meso-scale structure U_s relative to the mean flow of the mixture U_m. We borrow here an argument developed by Cholemari & Arakeri (2009) for turbulent flows driven by buoyancy: these authors argue that the velocity $(gL\delta\rho/\rho)^{1/2}$ corresponds to the 'free fall' velocity that a coherent region of density $\rho + \delta\rho$ sinking (or creaming) in a medium of density ρ reaches after a distance L, and L is such that the flow becomes uncorrelated at distances of order L. That 'fall velocity' corresponds to $U_s - U_m$. For a meso-scale structure, $\delta\rho$ is the difference in density between the structure and its surroundings.

In bubble columns, the density of meso-scale structures is $(1 - \varepsilon_{structure})\rho_L$, where $\varepsilon_{structure}$ denotes the void fraction averaged at the scale of the meso-scale structure. Meanwhile, the mean density of the two-phase mixture is $(1 - \varepsilon)\rho_L$. Hence, $\delta\rho/\rho_L = (\varepsilon - \varepsilon_{structure})$, meaning that the difference in density is proportional to the excess or to the deficit of void fraction in the structure compared with the mean

void fraction ε in the surrounding medium. Typically, clusters – that are gas dominated regions – would have an upward directed (i.e. positive) relative velocity with respect to the mean flow of the gas–liquid mixture of the order of

$$U_{R\ cluster\text{-}mixture} = U_{cluster} - U_m = C_{cluster}(gL_{cluster}[\varepsilon_{cluster} - \varepsilon])^{1/2}, \tag{5.1}$$

where the prefactor $C_{cluster}$ is (*a priori*) of order one, while voids, that are liquid dominated regions, would have a downward directed (i.e. negative) relative velocity with respect to the mean flow of the gas–liquid mixture:

$$U_{R\ void\text{-}mixture} = U_{void} - U_m = -C_{void}(gL_{void}[\varepsilon - \varepsilon_{void}])^{1/2}, \tag{5.2}$$

where C_{void} is a prefactor of order unity. The same reasoning can be applied to intermediate regions, so that the magnitude of the velocity between intermediate regions and the mixture obeys

$$U_{R\ int\text{-}mixture} = U_{int} - U_m = C_{int}(gL_{int}[\varepsilon_{int} - \varepsilon])^{1/2}, \tag{5.3}$$

again with a prefactor C_{int} of order unity. A positive sign has been retained for (5.3) because, according to figure 7, the mean void fraction in intermediate regions ε_{int} is slightly larger than the local void fraction ε when in the heterogeneous regime (the opposite holds in the homogeneous regime).

Equations (5.1)–(5.3) connect the relative velocity between a meso-scale structure and the mixture with the meso-scale structure characteristics in terms of size and concentration. The relevance of the propositions (5.1)–(5.3) is tested in the next section. For that, all the necessary information for evaluating the quantities $L_s[\varepsilon_s - \varepsilon]$ is available from experiments (see § 3). We also need to connect the relative velocity $U_s - U_m$ between a meso-scale structure and the mixture with the conditional relative bubble velocity $V_{b|s} - V_L$ which is a quantity directly accessible to measurements.

5.1. *Test of the relevance of the scaling proposed for the meso-scale structure relative velocity*

Concerning the quantities $L_s[\varepsilon - \varepsilon]$, and as all the data exploited here have been collected on the column axis, the local void fraction ε for the mixture is equal to ε_{axis}. The mean values $\langle L_{void}[\varepsilon_{void} - \varepsilon]\rangle$, $\langle L_{cluster}[\varepsilon_{cluster} - \varepsilon]\rangle$ and $\langle L_{int}[\varepsilon_{int} - \varepsilon]\rangle$ are shown versus V_{sg} in figure 11. All these quantities happen to remain fairly stable at large V_{sg}, say for V_{sg} above $\approx$10–15 cm s^{-1}. Note also that setting the minimum number of bubbles in clusters to one or to two does not induce any significant difference on $\langle L_{cluster}[\varepsilon_{cluster} - \varepsilon]\rangle$.

The last ingredient needed to test (5.1)–(5.3) is a connection between the mixture velocity U_m and the mean liquid velocity V_L. By definition, U_m is the mixture volumetric flux, that is, the velocity of the centre of volume of both phases (Ishii 1975). Therefore, U_m is related to unconditional phasic velocities by $U_m = (1 - \varepsilon)U_L + \varepsilon V_G$, and $U_m - V_L$ writes

$$U_m - V_L = \varepsilon(V_G - V_L) = \varepsilon U_R. \tag{5.4}$$

The prefactors $C_{structure}$ in (5.1)–(5.3) can now be evaluated. Indeed, for each meso-scale structure, one has

$$U_{R\ structure\text{-}mixture} = U_s - U_m = U_s + V_L - V_L - U_m = V_{b|s} - V_L - \varepsilon U_R. \tag{5.5}$$

Note that, in the last equality of (5.5), U_s has been identified with $V_{b|s}$. Strictly speaking, these two quantities are not the same as $V_{b|s}$ represents the mean velocity of bubbles within

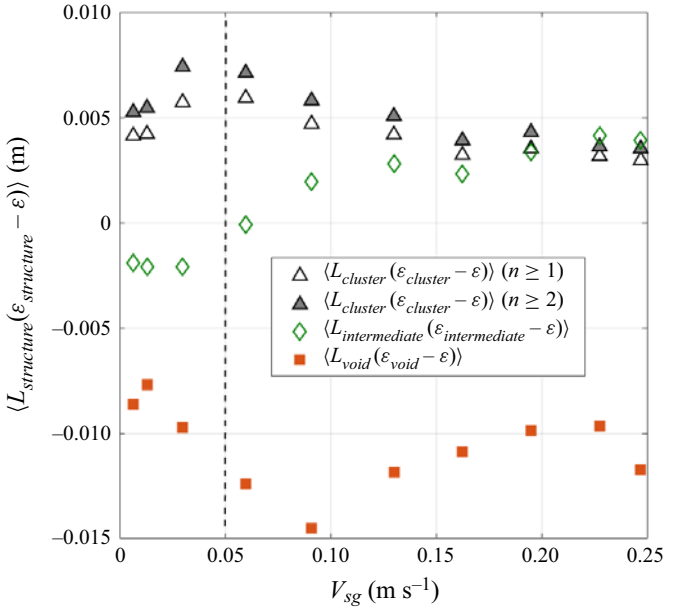

Figure 11. Evolution of the products $\langle L_{cluster}[\varepsilon_{cluster} - \varepsilon]\rangle$ for $n \geq 1$ and for $n \geq 2$, $\langle L_{int}[\varepsilon_{int} - \varepsilon]\rangle$ and $\langle L_{void}[\varepsilon_{void} - \varepsilon]\rangle$ with V_{sg}. Measurements performed in a $D = 0.4$ m column, on the column axis at $H/D = 3.625$.

the structure considered while, as discussed in the introduction of § 5, U_s corresponds to the velocity of the whole coherent region forming the structure meaning that U_s includes information on both gas and liquid phases. In clusters, owing to their large void fraction in the heterogeneous regime (see figure 7*c*), it is reasonable to assume that both phases move at nearly the same velocity and hence that $U_{clusters} \sim V_{b|clusters}$. A similar argument could be put forward for intermediate regions when V_{sg} is large. For void regions, experience shows that $V_{b|voids}$ and V_L nearly coincide when in the heterogeneous regime (see figure 9). Hence, assuming $U_s \sim V_{b|s}$ seems reasonable (to confirm that, liquid velocity measurements conditioned by the local gas concentration would be useful), and (5.5) combined with (5.1), (5.2) or (5.3) provides an estimate of the prefactor C_s, namely,

$$C_s = U_{R\ structure\text{-}mixture}/(gL_s|\varepsilon_s - \varepsilon|)^{1/2}, \tag{5.6}$$

where the denominator is known from figure 11. The values C_s deduced from (5.6) are given as a function of V_{sg} in figure 12. They all tend to nearly constant values at large V_{sg}: the mean values of C_s in the heterogeneous regime are provided in table 4; all these figures are almost insensitive to the range of V_{sg} selected to compute the average.

Moreover, all prefactors are of order unity, with $C_{cluster} \sim 3$, $C_{int} \sim 1.2$ and $C_{void} \sim -0.36$. The scalings proposed in (5.1)–(5.3) are therefore consistent, and these models provide the correct magnitude of the relative velocity of meso-scale structures with respect to the mixture. These results also confirm that the dynamics of these meso-scale structures is indeed controlled by a buoyancy–inertia equilibrium applied at their respective scales.

Here, each conditional bubble relative velocity $V_{b|s} - V_L$ has been connected with the characteristics of the corresponding meso-scale structure. Hence, thanks to (4.1), the unconditional bubble relative velocity is related with the characteristics of all three meso-scale structures present in the flow, combined with the repartition of bubbles

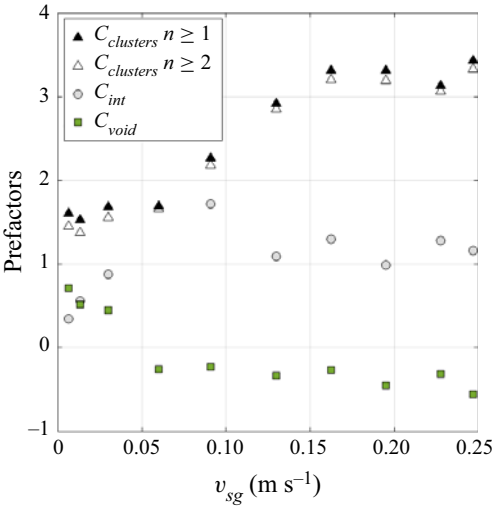

Figure 12. Evolution of the prefactors $C_{cluster}$, C_{int} and C_{void} deduced form (5.6) combined with (5.1)–(5.3) with V_{sg}.

between these three populations. This result demonstrates that the enhancement of the bubble relative velocity observed in the heterogeneous regime is the direct consequence of the collective dynamics occurring in these buoyancy-driven bubbly flows when the gas fraction is large enough.

5.2. *Scaling of the mean relative velocity: discussion*

At this stage, it is worthwhile to come back to the scaling of the relative velocity of (2.1) that involves the reference velocity $(gD\varepsilon)^{1/2}$ identified by Mezui *et al.* (2022). Let us first recall that (2.1) arises from scaling laws for mean velocities of both phases that have been corroborated over a large range of column diameters and flow conditions. However, direct measurements of the relative velocity in the heterogeneous regime such as those presented in § 2 are absent from the literature, so that the dependency of the relative velocity with the column diameter predicted by (2.1) cannot be directly tested from the available data. Similarly, the analysis in terms of meso-scale structures developed above concerns but a single column diameter, and more experiments are required to further investigate meso-scale structure characteristics. Yet, as shown in Mezui *et al.* (2022), the existence of an asymptotic heterogeneous state at large V_{sg} is supported by many experiments performed in various column diameters and flow conditions. The presence of such an asymptotic behaviour prompted us to rescale the relative velocities $U_{R\ structure\text{-}mixture}$ using D as the relevant scale for the dimensions L_s of meso-scale structures and using the gas hold-up ε for scaling the differences in concentration $[\varepsilon_s - \varepsilon]$. Table 5 provides L_s/D, $[\varepsilon_s - \varepsilon]/\varepsilon$ and the quantity $\langle gL_s[\varepsilon_s - \varepsilon]\rangle^{1/2}/(gD\varepsilon)^{1/2}$ that enter (5.1)–(5.3). The last line of table 5 provides for each structure the relative velocities $U_{R\ structure\text{-}mixture}$ scaled by the velocity $(gD\varepsilon)^{1/2}$; the resulting coefficients are comprised between 0.1 and 0.6; such $O(1)$ values seem reasonable.

The scaling for the unconditional relative velocity $U_R = V_G - V_L$ can be deduced from the above information. Starting from (4.2) and still assuming that $U_s = V_{b|s}$, we have $U_R = N_{clusters}(U_{clusters} - U_m) + N_{int}(U_{int} - U_m) + N_{voids}(U_{voids} - U_m) + \varepsilon U_R$ that transforms

https://doi.org/10.1017/jfm.2023.259 Published online by Cambridge University Press

Measured $U_{R\ structure\text{-}mixture}/(gL_{structure}[\varepsilon_{structure}-\varepsilon])^{1/2}$	$C_{cluster}$ Dense regions $n \geq 1$, (5.1)	$C_{cluster}$ Dense regions $n \geq 2$, (5.1)	C_{int} Intermediate regions, (5.3)	C_{void} Void regions, (5.2)
Average prefactor for $V_{sg} \geq 6\,\mathrm{cm\,s^{-1}}$	2.87	2.78	1.26	−0.34
Average prefactor for $V_{sg} \geq 9\,\mathrm{cm\,s^{-1}}$	3.06	2.97	1.26	−0.36
Average prefactor for $V_{sg} \geq 13\,\mathrm{cm\,s^{-1}}$	3.22	3.13	1.17	−0.38

Table 4. Mean values of prefactors C_s in the heterogeneous regime when assuming $U_s = V_{b|s}$.

Mean values evaluated for $V_{sg} \geq 9\,\mathrm{cm\,s^{-1}}$	Clusters with $n \geq 1$	Clusters with $n \geq 2$	Intermediate regions	Void regions
Mean size	0.018 m	0.022 m	0.062 m	0.074 m
Mean size / D	0.045	0.054	0.155	0.185
$\langle(\varepsilon_{structure} - \varepsilon)/\varepsilon\rangle$	0.464	0.585	0.054	−0.42
$\langle gL_{structure}[\varepsilon_{structure} - \varepsilon]\rangle^{1/2}/(gD\varepsilon)^{1/2}$	0.17	0.19	0.15	−0.3
$C_{structure}$ (from table 4)	3.06	2.97	1.26	−0.36
Prefactor $U_{R\ structure\text{-}mixture}/(gD\varepsilon)^{1/2}$	0.520	0.564	0.189	−0.108

Table 5. Average characteristics of meso-scale structures in the heterogeneous regime measured on the axis of a $D = 0.4$ m bubble column and at $H/D = 3.625$, pre-factors $C_{structure}$ and ratio $U_{R\ structure\text{-}mixture}/(gD\varepsilon)^{1/2}$.

into

$$\begin{aligned}(1-\varepsilon)U_R &= N_{clusters}(U_{clusters} - U_m) + N_{int}(U_{int} - U_m)\\ &+ N_{voids}(U_{voids} - U_m) = (N_{clusters}\left[(U_{clusters} - U_m)/(gD\varepsilon)^{1/2}\right]\\ &+ N_{int}\left[(U_{int} - U_m)/(gD\varepsilon)^{1/2}\right]\\ &+ N_{voids}\left[(U_{voids} - U_m)/(gD\varepsilon)^{1/2}\right])(gD\varepsilon)^{1/2} = C_R(gD\varepsilon)^{1/2}. \end{aligned} \tag{5.7}$$

The prefactor C_R has been evaluated over various ranges of V_{sg} within the heterogeneous regime: it is given in table 6 where we have also considered the two options for clusters (namely $n \geq 1$ and $n \geq 2$). Overall, the dispersion is small, and one gets

$$(1-\varepsilon)U_R \sim 0.30 \pm 0.01(gD\varepsilon)^{1/2}. \tag{5.8}$$

As the void fraction in the heterogeneous regime ranges from 20 to 37 % for the experimental conditions considered here, the ratio $U_R/(gD\varepsilon)^{1/2}$ evolves from 0.37 to 0.50, to be compared with the value $U_R \sim 0.41(gD\varepsilon)^{1/2}$ deduced from direct velocity measurements (see (2.1)). The difference between these two results remains in the interval [−11 %; +23 %]. Such a difference is quite acceptable owing to the variety of independent measurements involved in that analysis (the latter include void fraction, unconditional and conditional relative velocities, statistics on size and on concentration for the three meso-scale structures, repartition of bubbles among these structures based on Voronoï tessellations) and possibly also owing to the assumption $U_s \approx V_{b|s}$ we made.

The expression of the relative velocity from (2.1) derived from scaling considerations is recovered here using the partition of bubbles into three distinct populations. Again, and as seen in § 4, (5.7) and (5.8) show that the increase of the bubble relative velocity beyond the terminal velocity value originates from the dynamics of the meso-scale structures present in the heterogeneous regime. In this process, clusters bring the strongest contribution. Thanks to the significant proportion of bubbles they gather (table 1) and thanks to their high relative velocity with respect to the mixture (clusters correspond to the largest ratio $U_{R\ structure\text{-}mixture}/(gD\varepsilon)^{1/2}$ in table 5), they contribute 65–68 % to U_R. Intermediate regions host the majority of bubbles but their relative velocity with respect to the mixture is approximately three times smaller than that of clusters: they contribute 33–35 % to U_R. Last, void regions are sinking in the mixture: they carry few bubbles and their (negative) contribution to U_R is almost negligible (∼2 %).

https://doi.org/10.1017/jfm.2023.259 Published online by Cambridge University Press

$U_{R\ structure\text{-}mixture}/(gD\varepsilon)^{1/2}$	Cluster $n \geq 1$	Cluster $n \geq 2$	Intermediate regions	Void regions	$(1-\varepsilon)/(gD\varepsilon)^{1/2}$ $n \geq 1$	$(1-\varepsilon)/(gD\varepsilon)^{1/2}$ $n \geq 2$
mean value over the range $V_{sg} \geq 6\,\mathrm{cm\,s^{-1}}$	0.517	0.556	0.176	−0.105	0.292	0.307
mean value over the range $V_{sg} \geq 9\,\mathrm{cm\,s^{-1}}$	0.520	0.564	0.189	−0.108	0.300	0.317
mean value over the range $V_{sg} \geq 13\,\mathrm{cm\,s^{-1}}$	0.515	0.563	0.187	−0.110	0.297	0.315

Table 6. Prefactors for the relative velocities $U_{R\ structure\text{-}mixture}$ and for the unconditional relative velocity U_R with respect to the velocity scale $(gD\varepsilon)^{1/2}$ in the heterogeneous regime (from measurements on the axis of a $D = 0.4\,\mathrm{m}$ bubble column at $H/D = 3.625$).

Although data are still lacking to directly examine how the relative velocity evolves with the column diameter, (5.7) and (5.8) provide an indirect way to discuss the dependency of U_R on D. According to experiments, the void fraction weakly varies with D (in Mezui *et al.* (2022), the void fraction on the column axis is found to evolve as $D^{-0.2}$), so that (5.8) indicates that the relative velocity monotonously increases with D. At first sight, that prediction seems odd if one refers to a single bubble dynamic that is controlled by its interaction with the liquid at a scale commensurable with the bubble size, and not with the size of the domain. However, we have seen that collective dynamics in these buoyancy-driven bubbly flows plays a central role in the formation of meso-scale structures, and that the presence of both dense and dilute structures drives the momentum exchange between phases and leads to an enhancement of the relative velocity. Further, the various contributions $U_{R\ structure\text{-}mixture}$ appearing in (5.7) are directly related with the characteristics in terms of size and concentration that each meso-scale structure has in the asymptotic limit (i.e. in the limit of large V_{sg}). The question left is thus whether the scalings with D and with ε used to build table 5 are relevant or if they are artificial.

Concerning ε, an examination of the evolution of the coefficients C_s of figure 12 versus ε instead of V_{sg} indicates that a scaling with the void fraction is indeed acceptable for gas hold-up above approximately 30 %.

Regarding the dimensions of meso-scale structures, it is unlikely that the typical width of clusters grows with D, but the void regions do have an extension of order D. Such a statement is supported by our experiments in the $D = 0.4$ m column (figure 7). It is also sustained by the results presented in the next section where it is shown that void regions correspond to large-scale vorticity regions whose dimension is of order D.

5.3. *Flow structure in the heterogeneous regime*

Concerning the internal structure of the flow in the heterogeneous regime, the spatial organisation of the gas phase deduced from 1-D Voronoï tessellations has already demonstrated the presence of thin regions at high void fractions, and of large regions at low void fractions. When examining the flow through column walls using direct lightning, these void regions correspond to dark zones (figure 13) while bright regions indicate a significant presence of bubbles (whose interface reflects light back towards the observer). These dark regions seem to correspond to the large-scale vortical-like structures that have often been reported in the literature (and that are illustrated in the video enclosed as supplementary material associated with the reference Mezui *et al.* 2022).

To quantify such vortical structures, we exploited the local liquid velocity provided by a Pavlov tube. Spatial correlations were not accessible with a single sensor, and liquid velocity measurements conditioned by the local gas concentration were not attempted. Instead, we considered time series collected from a single Pavlov tube even though its temporal resolution was limited (approximately 20 Hz, see Mezui *et al.* (2023) for further details).

The zero crossings of the signal $v_L(t) - V_L$ were detected and the density of zero crossing n_s per unit length was evaluated using the mean liquid velocity to transform time into space. The resulting characteristic length scale n_s^{-1} provides the mean vertical size of vortical structures. Let us mention that, for a turbulent single-phase flow, Liepmann & Robinson (1953) related the Taylor microscale λ to the average distance n_s^{-1} between zero crossings of a streamwise velocity signal of a turbulent flow, and they show that $n_s^{-1} = B\lambda$, where B is a constant that accounts for intermittency ($B = \pi$ for a Gaussian time series with also a Gaussian derivative). In our case, it is not clear if the vertical spatial scale we construct is related to any turbulence scale, as we are far from the conditions

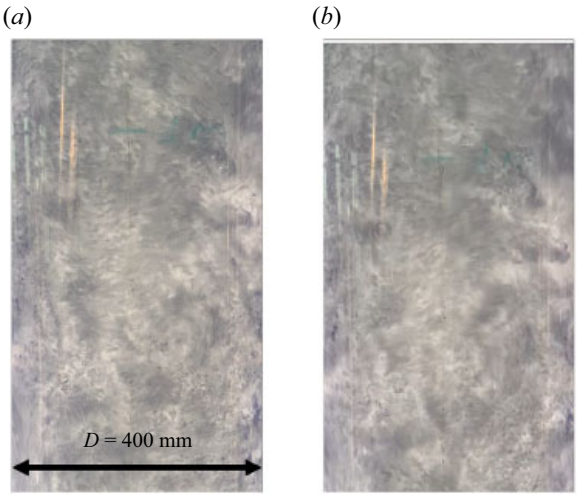

Figure 13. Images of flow near column walls in the heterogeneous regime. Bright zones indicate the presence of many bubbles while dark zones correspond to structures comprising few bubbles. The vertical extent of the images corresponds to sections at 0.8 and at 2 metres above gas injection ($D = 0.4$ m, static liquid height = 2 m). Movies are included in the supplementary material of Mezui *et al.* (2022).

of homogeneity and isotropy required by the model from Liepmann & Robinson. From measurements in the $D = 0.4$ m column, n_s^{-1} was found equal to D (within 10 %) for V_{sg} larger than $\approx 10\,\mathrm{cm\,s^{-1}}$. Although acquired in a single column, this result supports the idea that the size of vortical structures does scale as the bubble column diameter. A few other results on the integral length scale of turbulence (Mezui *et al.* 2023) and on the size of vortical structures in various bubble columns (Cartellier 2019) also indicate that D is the relevant scale.

In parallel, let us show that the regions containing bubbles are not in the form of 'compact' clusters of bubbles. Indeed, the high particle Reynolds number bubbles considered here (see § 2) are in a constant drag coefficient regime (when isolated). If one considers a compact, close to spherical assembly of N such bubbles, the dynamics of that ensemble would be also governed by a constant drag coefficient, and its relative velocity would be equal to $N^{1/6}U_T$. Therefore, the relative velocities between approximately $2U_T$ and $2.5U_T$ that we measured in heterogeneous conditions at large V_{sg} (for V_{sg} above $10\,\mathrm{cm\,s^{-1}}$, as discussed in § 2), would be recovered with $N = 64$ for $2U_T$, or with $N = 244$ for $2.5U_T$: these figures are 10 to 50 times larger than the average number of bubbles detected in clusters (figure 7). Clearly, the existence of compact assemblies of bubbles does not correspond to observations. The question is now how thin bubbly 'sheets' could induce such an enhancement of the bubble relative velocity.

From these findings, a tentative cartoon of the spatial organisation of phases in the heterogeneous regime emerges: bubbles accumulate in narrow (a few bubbles in size) regions located in between large (typically $\approx 0.2D$ according to figure 7*b*) vortical structures that are almost free of bubbles. This situation is sketched in figure 14. The dense regions containing most bubbles are like thin 'sheets' or 'curtains' (a few bubble diameter wide) located in between vortices whose extent is of order D. Thus, these arguments combined with (5.7) support a relative velocity controlled by the lateral dimension of the column.

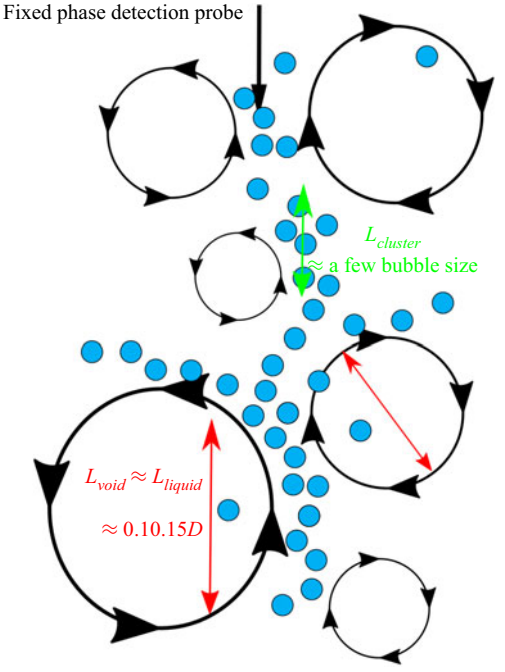

Figure 14. Tentative sketch of the flow organisation. As it can be appreciated in the movies included as supplementary material in Mezui *et al.* (2022) (see figure 13), large vortical liquid structures are seen as dark zones (as they comprise few bubbles), while clusters of bubbles correspond to bright zones. Such large dark vortices, that are almost free of bubbles, show bubble 'curtains' between them. Although collected near the walls, these structures can be seen as representative of the internal flow structures inside the column.

To conclude, in this section, the relative velocity observed in the heterogeneous regime has been connected with the characteristics in terms of size and concentration of dense, intermediate and dilute regions formed in these buoyancy-driven bubbly flows. These meso-scale structures and the dynamics they induce are believed to be at the origin of the swarm factor introduced in Eulerian two-fluid simulations to evaluate the momentum exchange between phases in the heterogeneous regime. Moreover, a number of experimental results support the existence of an asymptotic flow organisation at large V_{sg}, in particular, with the saturation of the gas concentration in dense regions, and with limiting values of the spatial extent of meso-scale structures. Additional investigations are required to fully determine how these asymptotic values evolve with parameters, and in particular with the column diameter. Let us finally underline that, in their simulations of heterogeneous conditions, Panicker, Passalacqua & Fox (2020) captured the presence of bubble swarms with a characteristic length scale of order V_G^2/g and predicted a significant increase of the mean gas velocity compared with homogeneous conditions: these findings are consistent with the experimental results presented here.

6. Velocity fluctuations, internal structure and fast-track mechanism

So far, we have discussed the scalings of the mean transport velocity and of relative velocities. Let us consider now velocity fluctuations. Mezui *et al.* (2022) found that the unconditional standard deviations of liquid velocity V'_L and of bubble velocity V'_G evolve as $(gD\varepsilon)^{1/2}$, but these results were mostly validated for a single bubble column diameter.

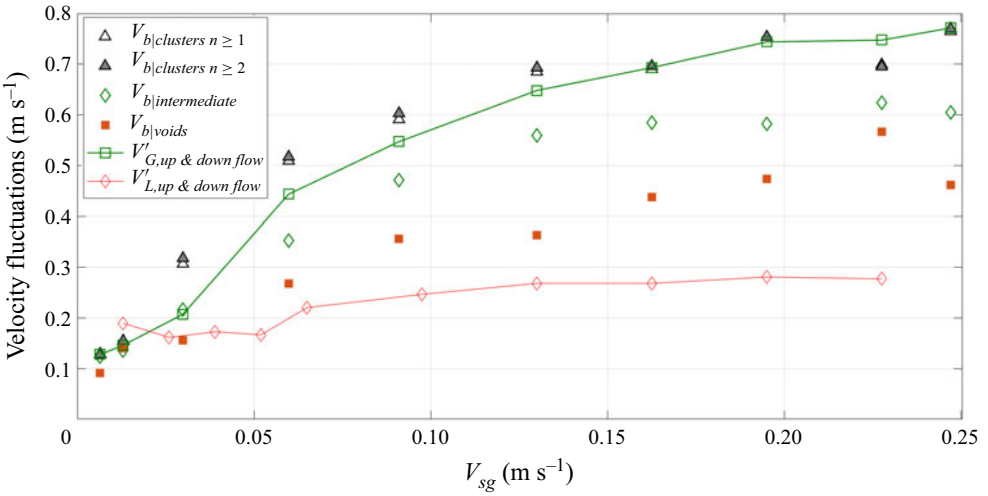

Figure 15. Standard deviations std($v_{b|s} - V_G$) of bubble velocity conditioned by meso-scale structures i.e. clusters, intermediate and void regions with respect to the unconditional mean bubble velocity V_G versus the gas superficial velocity. Comparison with unconditional standard deviations of liquid and gas velocities. Measurements performed in a $D = 0.4$ m column, on the column axis at $H/D = 3.625$.

Before discussing the possible origin of such a scaling, let us analyse the experimental data gathered on the axis of the $D = 0.4$ m column. As before, we take advantage of the Doppler probe to examine the behaviour of the standard deviation of the bubble velocity conditional to meso-scale structures. Using the mean unconditional bubble velocity V_G as the reference, we evaluated the standard deviation $V'_{b|s} = \mathrm{std}(v_{b|s} - V_G)$, where std denotes the standard deviation and $v_{b|s}$ is the instantaneous bubble velocity in the selected structure, shown in figure 15 for clusters, intermediate regions and void regions. Their evolutions of the quantities $v_{b|s}$ with V_{sg} have qualitatively the same allure as those of mean conditional velocities $V_{b|s}$ shown in figure 9. Notably, the differences between meso-scale structures remain small when in the homogeneous regime and increase when in the heterogeneous regime. In the latter regime, the difference from one structure to the other typically amounts to 0.1–0.2 m s^{-1}. Also, velocity fluctuations are larger in clusters than in intermediate regions, and are larger in intermediate regions than in void regions. These trends are not sensitive to the minimum number of bubbles in a cluster.

As for the mean velocity, the unconditional standard deviation of bubble velocity can be deduced from the contributions of the three meso-scale structures, weighted by the proportion of bubbles they contain. Indeed, the sum $N_{clusters}V'_{b|clusters} + N_{int}V'_{b|int} + N_{voids}V'_{b|voids}$ has been compared to the standard deviation V'_G, and the agreement is good with a discrepancy of at most 25 % in the homogeneous regime and at most 20 % in the heterogeneous regime. In the latter case, the contributions to velocity fluctuation mainly originate from clusters (42–45 % contribution) and from intermediate regions (51–55 % contribution) with a small remaining contribution (3–4 %) arising from void regions.

The fact that bubble velocity fluctuations are significantly larger than liquid velocity fluctuations in the heterogeneous regime has already been reported (Mezui *et al.* 2022). We show here that this is also true for conditional bubble velocities, with the exception of the very low V_{sg} limit that belongs to the homogeneous regime. This is not surprising owing to the overwhelming contributions of clusters and of intermediate regions to bubble velocity fluctuations in the heterogeneous regime. Oddly, this is even true in void regions,

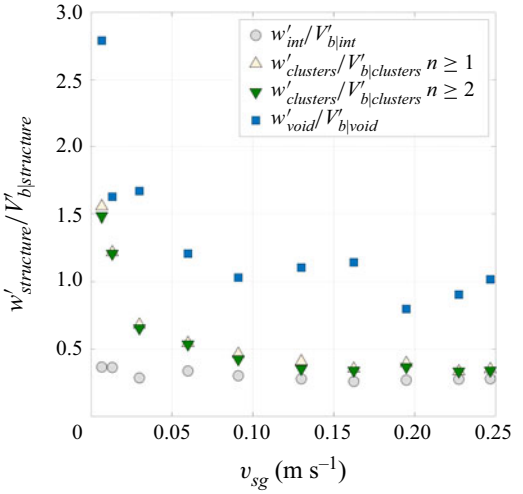

Figure 16. Comparison of the velocity variation $w'_{structure}$ due to size and concentration of meso-scale structures pertaining to the same population with bubble velocity fluctuations conditioned by meso-scale structures $V'_{b|structure}$. Measurements performed in a $D = 0.4$ m column, on the column axis at $H/D = 3.625$.

possibly because these statistics recover bubbles having quite diverse environments as the local void fraction typically ranges from 0.4 to 0.1 times the mean hold-up (see figure 3 and associated comments).

The fluctuations in bubble velocity arise from bubble velocity variations between different types of meso-scale structures. They can also arise from velocity variations between meso-scale structures belonging to the same population as both buoyancy and inertia are variable from one structure to the other. In an attempt to evaluate that second contribution, we considered the quantities $L_{structure}[\varepsilon_{structure} - \varepsilon]$ that enter (5.1)–(5.3) for the three meso-scale structures. Following the scaling rules given by (5.1)–(5.3), the velocity fluctuation associated with variations in size and concentration for a given meso-scale structure is evaluated as $w'_{structure} = gstd(L_{structure}[\varepsilon_{structure} - \varepsilon])^{1/2}$. These estimations are compared with the bubble velocity fluctuations conditioned by meso-scale structures in figure 16. The curves are rather stable for V_{sg} above 10–15 cm s^{-1}. It happens that $w'_{structure}/V'_{b|structure} \sim 3$ for clusters, 1.5 for intermediate regions and approximately 1 for void regions. The contribution of the variability in size and in concentration of structures is therefore small for clusters, and it remains moderate but still higher than unity for intermediate regions. Hence, as clusters and intermediate regions bring the largest contribution to fluctuations, a significant fraction of bubble velocity fluctuations is therefore related with the velocity differences between the various types of meso-scale structures. Owing to the key contribution of the latter, we develop hereafter the idea that a fast-track mechanism is at play and that it connects the relative velocity with bubble velocity fluctuations.

According to the presumed internal organisation of the flow in the heterogeneous regime as sketched in figure 14, a plausible mechanism could be the following. As bubbles are mainly located between vortices, a fast-track mechanism (similar to that observed in a turbulent flow laden with inertial particles Wang & Maxey 1993) takes place. Bubbles are channelling between vortices, and they preferentially pick up the side of eddies with an upward motion (choosing the downward side induces a much larger local relative velocity and hence a much larger drag). The result is a faster upward directed vertical

bubble velocity. Such a picture is consistent with the conditional velocity measurements presented above. It also provides a physical background to the swarm coefficient often introduced in simulations to force the drag on a bubble to decrease with the local void fraction.

Such a picture is also consistent with the impact a fast-track mechanism has on the enhancement of the relative velocity. Indeed, in turbulent flows laden with inert particles, the enhancement of the settling velocity of dense particles is found proportional to the velocity fluctuations of the background turbulence, with a prefactor typically between 0.1 and 0.5 depending on particle and on flow characteristics (see for e.g. Wang & Maxey 1993; Mora *et al.* 2021). Making a crude parallel with the present situation, we can consider V_L' as the magnitude of external velocity fluctuations. In § 3, we have seen that on the axis of a $D = 0.4$ m column, the liquid fluctuations scale as $V_L' \approx 0.22(gD\varepsilon)^{1/2}$ while the mean relative velocity scales as $U_R \approx 0.3$–$0.4(gD\varepsilon)^{1/2}$: these two results indicate that when in the heterogeneous regime, U_R and V_L' remain proportional with a ratio approximately 0.5–0.7. This finding is therefore consistent with what is known about the impact of a fast-track mechanism on the relative motion of inclusions with respect to a turbulent continuous phase. In addition, the velocity enhancement observed here is consistent with recent results concerning the frontier between enhancement and hindering (Mora *et al.* 2021): the Rouse number of inclusions $Ro = U_R/V_L'$, which lies here between 0.5 and 0.7, is indeed small enough to avoid the triggering of a loitering scenario.

A question left open at this stage is why bubbles remain (on average) accumulated and stuck in between large-scale liquid structures. This is a counter-intuitive organisation if one thinks of bubbles interacting with turbulent eddies in a denser fluid, as bubbles are preferentially moving towards low-pressure zones, i.e. in the core of eddies. Our belief is that the situation in bubble columns is not the same as that of bubbles immersed in a weak turbulent field. We have shown in § 2 that, in the heterogeneous regime, buoyancy is the source of the mean motion and of velocity fluctuations by way of internal density gradients. In such flows, the accumulation or the depletion of bubbles are not governed by eddies interacting with independent, quasi-isolated bubbles, but by collective dynamics that imposes its forcing on the more inert phase. In other words, a local bubble accumulation induces an upwelling motion that must be compensated by a nearby downward motion of an essentially liquid (possibly including a few bubbles) zone. This is why, once formed, the (thin) clusters of bubbles as well as the empty regions are believed to persist for some time which is long enough compared with the transit time of the mixture from the bottom to the top of the bubble column. In our experiments, that transit time is approximately 1.5–3 s in the heterogeneous regime, and it is indeed small compared with the bubble response time a^2/ν_L that is approximately 10 s here. In other words, for the flow conditions considered here, there is not enough time available for bubbles to be significantly dispersed or to significantly diffuse outside dense regions. Note that similar dynamics have been reported in experiments (Kimura & Iga 1995) and in simulations (Climent & Magnaudet 1999; Nakamura *et al.* 2020) of micro-bubbles-induced convection in shallow conditions with the formation of mushrooms similar to those arising in Rayleigh–Taylor instability.

The proposed scenario deserves to be tested further using experiments and/or direct numerical simulations. This scenario is also expected to change when considering different flow conditions, notably in terms of coalescence efficiency. As a crude quantification of the limit of validity of this scenario, let us evaluate the size that would have bubbles so that their terminal velocity (when isolated) equals the relative velocity we measured in the $D = 0.4$ m column. For a relative velocity approximately $2U_T$ where $U_T \approx 0.21$–$0.23\ \mathrm{m\,s^{-1}}$, the bubble diameter should be multiplied by $44^{1/3} \approx 3.5$ compared with the size of the

bubbles we considered. For a relative velocity approximately $2.5U_T$, the multiplication factor would be $244^{1/3} \approx 6$. Hence, we expect the proposed scenario to be modified when bubbles above 20 to 40 mm in equivalent diameter start to appear in the flow. Such a limit also corresponds to bubbles whose terminal velocity, approximately 0.5–0.7 m s^{-1}, would become comparable to the magnitude of velocity fluctuations at large V_{sg} in a $D = 0.4$ m column. In other words, the Rouse number of such bubbles would become of order one or above, and loitering could occur instead of fast track, and that may possibly lead to a decrease in the relative velocity (Mora *et al.* 2021). Pushing the limit even further, for bubble size of the order of D (as observed for example in fluidised beds), the dynamic would drastically change as one approaches slug flows.

7. Conclusions

We report experimental results of the hydrodynamics of bubble columns operated in the heterogeneous regime. The reactor was operated in controlled conditions by focusing on variables conditioned by the local void fraction. Experiments in a $D = 0.4$ m air–water bubble column were performed with bubbles in the wobbling regime. Furthermore, in our experimental conditions, the bubbles presented no significant coalescence.

In a first step, the concentration field at small scales and its connection with the relative motion between phases has been investigated for gas superficial velocities up to 25 cm s^{-1}. From Voronoï tessellations in one dimension built from the signal delivered by an optical probe, the homogeneous/heterogeneous transition has been shown to correspond to a standard deviation of the probability density of Voronoï cell width that levels off from its value for an RPP. The departure from an RPP allows to unambiguously identify meso-scale structures, namely clusters (i.e. regions where bubbles tend to accumulate), void regions (i.e. liquid regions including few bubbles) and intermediate regions. These meso-scale structures have been characterised in terms of size and of concentration. In the heterogeneous regime, size and concentration p.d.f.s seem to asymptote as V_{sg} increases. In particular, the mean size of these meso-scale structures tends towards constant values for V_{sg} higher than $\approx$0.1 m s^{-1}. Also, the absolute concentration in clusters saturates to 45–50 %, while the concentration in voids and in intermediate regions slightly but continuously increases with the mean gas hold-up. The picture that comes out from conditional measurements using optical probes and from Pavlov tubes comprises void regions that correspond to vortices in the liquid those size is a fraction of D and 'thin' clusters – typically a few bubbles wide – structured as sheets in between these vortices. This picture is consistent with a fast-track mechanism that, for moderate Rouse numbers, leads to liquid velocity fluctuations that are a fraction of the relative velocity between phases.

The origin of the large relative velocity observed in the heterogeneous regime has been, for a long time, a central question in the hydrodynamics of bubble columns. A series of arguments demonstrating the key role of meso-scale structures on the relative velocity of bubbles has been presented as follows.

(i) Direct measurements of the unconditional mean relative velocity show that the relative velocity levels off at the homogeneous–heterogeneous transition. In addition, the relative velocity asymptotes at large V_{sg}: the limit, in the $D = 0.4$ m column, is approximately 2.4 times the terminal velocity of bubbles.

(ii) Bubble velocity measurements conditional upon the local gas concentration indicate that bubbles in clusters are moving up much faster, up to 3 to 3.5 times the terminal velocity, than bubbles in void regions whose speed is nearly equal to the

unconditional liquid velocity. Similarly, bubbles in intermediate regions are moving up faster, up to 1.5 to 2 times the terminal velocity, than bubbles in void regions.

As the mean unconditional relative velocity of bubbles is recovered from conditional mean relative velocities weighted by the proportion of bubbles present in each meso-scale structure, these findings demonstrate that the flow dynamics in the heterogeneous regime originates from collective effects linked with the apparition of meso-scale structures.

In addition, by assuming equilibrium between inertia and buoyancy at the scale of each meso-scale structure, we show that the velocity of each meso-scale structure relative to the mixture is related to its characteristics in terms of size and concentration. Consequently, the unconditional mean bubble relative velocity has been related with the characteristics of all three meso-scale structures present in the flow. Such result opens the way to the identification of the proper scaling of the relative velocity. In particular, the spatial extension of void regions seems to be proportional to the bubble column diameter, a feature that could explain why the relative velocity evolves as $(gD\varepsilon)^{1/2}$ as indicated by unconditional measurements. These conjectures need to be tested over a wider range of conditions. In particular, the impact of bubble column diameters on the relative velocity and meso-scale structures need to be investigated. For instance, by examining higher gas superficial velocities, it would be worthwhile to identify what controls the limits in concentration of meso-scale structures.

Funding. The LEGI is part of the LabEx Tec21 (Investissements d'Avenir – grant agreement no. ANR-11-LABX-0030). That research was also partially funded by IDEX UGA (no. ANR-15-IDEX-0002).

Declaration of interests. The authors report no conflict of interest.

Author ORCIDs.
M. Obligado https://orcid.org/0000-0003-3834-3941;
A. Cartellier https://orcid.org/0000-0002-1522-5048.

Appendix A. Evaluation of the gas concentration in a Voronoï cell

A.1. *Connection between cell width and cell concentration*

The magnitude of ΔT_k is related to the local and instantaneous concentration, that is, the concentration at the scale of the kth Voronoï cell. A large ΔT_k means that neighbouring bubbles are far from the test bubble, or equivalently that the concentration in the vicinity of the test bubble is low. Inversely, a small ΔT_k indicates the presence of close neighbours, that is, a high void fraction in the vicinity of the test bubble.

Raimundo *et al.* (2019) argued that the quantity $\Delta T_k/\langle \Delta T\rangle$ equals the ratio of the local and instantaneous gas concentration ε_k to the average gas hold-up ε at the measuring location, i.e. $\Delta T_k/\langle \Delta T\rangle = \varepsilon/\varepsilon_k$. This equality must be replaced by (A1) below. Indeed, let us consider N bubbles detected over a measuring duration T_{probe}. By definition, the void fraction ε equals $(\sum_i t_{gi})/T_{probe}$, where i goes from 1 to N. By construction, the Voronoï cells map all the space (that is, the whole measuring duration) so that $T_{probe} = \sum_k \Delta T_k$, where k goes from 1 to N. Hence, $\varepsilon = (\sum_i t_{gi})/T_{probe} = (\sum_i t_{gi})/\sum_k \Delta T_k = N\langle t_g\rangle/[N\langle \Delta T\rangle]$, where mean values have been introduced in the last equality. Meanwhile, the local void fraction ε_k (i.e. at the scale of the kth cell) is $t_{gk}/\Delta T_k$. Therefore,

$$\varepsilon_k/\varepsilon = \left[t_{gk}/\Delta T_k\right] / \left[\langle t_g\rangle/\langle \Delta T\rangle\right] = \left[t_{gk}/\langle t_g\rangle\right] / \left[\langle \Delta T\rangle/\Delta T_k\right]. \tag{A1}$$

The concentration ε_k in the kth cell scaled by the local concentration ε is indeed proportional to $\langle \Delta T\rangle/\Delta T_k$, but these quantities are not equal. The proportionality

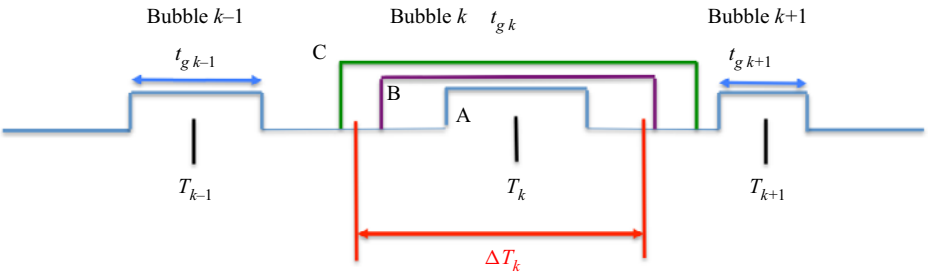

Figure 17. Void fraction at the scale of a Voronoï cell.

coefficient happens to depend on the gas residence time t_{gk} divided by the mean gas residence time $\langle t_g \rangle$. The coefficient changes from one bubble to another in a given record. Therefore, it is not possible to univocally transform a threshold in $\Delta T_k/\langle \Delta T \rangle$ (such a threshold is used to distinguish the three populations, namely clusters, voids and intermediate regions) into a threshold in terms of cell concentration. Instead, the distributions of actual concentrations in each population need to be analysed (see figure 4 and related text).

A.2. *Gas concentration in a Voronoï cell*

Here above, the void fraction ε_k at the scale of the kth cell is estimated as $t_{gk}/\Delta T_k$. The formula is exact for the situation of the bubble indicated as A in figure 17. Let us consider the three successive bubbles $k-1$, k and $k+1$. Let us increase the residence time of bubble k while maintaining everything else fixed. In particular, the centres of the three bubbles remain located at T_{k-1}, T_k and T_{k+1}, so that the kth Voronoï cell keeps its width ΔT_k. When the kth bubble grows and reaches the situation B (figure 17), the right-hand side of the gas residence interval becomes located outside the cell. When the bubble grows further and reaches the situation C (figure 17), the residence time of the bubble k exceeds the Voronoï cell width and ε_k becomes larger than unity. Hence, the formula $t_{gk}/\Delta T_k$ becomes incorrect when dealing with large bubbles (large t_{gk}) in a dense surrounding (small ΔT_k). In practice, one should account only for the fraction of the gas residence located inside the Voronoï cell. In § 5, we used a somewhat crude correction as we simply set $\varepsilon_k = 1$ whenever $t_{gk}/\Delta T_k$ exceeded unity. However, the number of events concerned by that issue is quite limited (it is always less than 12 % of the population) so that this approximation does not affect the trends identified nor the mean values.

References

Besagni, G., Inzoli, F. & Ziegenhein, T. 2018 Two-phase bubble columns: a comprehensive review. *Chem. Engng* **2** (2), 13.

Cartellier, A.H. 2019 Bubble columns hydrodynamics revisited according to new experimental data. In *Recent advances in bubble columns organized by EFCE and SFGP*.

Cholemari, M.R. & Arakeri, J.H. 2009 Axially homogeneous, zero mean flow buoyancy-driven turbulence in a vertical pipe. *J. Fluid Mech.* **621**, 69–102.

Climent, E. & Magnaudet, J. 1999 Large-scale simulations of bubble-induced convection in a liquid layer. *Phys. Rev. Lett.* **82** (24), 4827.

De Nevers, N. 1968 Bubble driven fluid circulations. *AIChE J.* **14** (2), 222–226.

Ferenc, J.-S. & Néda, Z. 2007 On the size distribution of poisson voronoi cells. *Physica* A **385** (2), 518–526.

GEMELLO, L., CAPPELLO, V., AUGIER, F., MARCHISIO, D. & PLAIS, C. 2018 CFD-based scale-up of hydrodynamics and mixing in bubble columns. *Chem. Engng Res. Des.* **136**, 846–858.

ISHII, M. 1975 Thermo-fluid dynamic theory of two-phase flow. *NASA Sti/recon Tech. Rep.* A **75**, 29657.

ISHII, M. & ZUBER, N. 1979 Drag coefficient and relative velocity in bubbly, droplet or particulate flows. *AIChE J.* **25** (5), 843–855.

JOSHI, J.B., PARASU, U.V., PRASAD, C.V.S., PHANIKUMAR, D.V., DESHPANDE, N.S. & THORAT, B.N. 1998 Gas hold-up structures in bubble column reactors. *Proc. Indian Natl Sci. Acad.* **64** (4), 441–567.

KANTARCI, N., BORAK, F. & ULGEN, K.O. 2005 Bubble column reactors. *Process Biochem.* **40** (7), 2263–2283.

KIKUKAWA, H. 2017 Physical and transport properties governing bubble column operations. *Intl J. Multi-phase Flows* **93**, 115–129.

KIMURA, R. & IGA, K. 1995 Bubble convection. *Mixing Geophys. Flows* **749**, 35–51.

KRISHNA, R., WILKINSON, P.M. & VAN DIERENDONCK, L.L. 1991 A model for gas holdup in bubble columns incorporating the influence of gas density on flow regime transitions. *Chem. Engng Sci.* **46** (10), 2491–2496.

LEFEBVRE, A., MEZUI, Y., OBLIGADO, M., GLUCK, S. & CARTELLIER, A. 2022 A new, optimized doppler optical probe for phase detection, bubble velocity and size measurements: investigation of a bubble column operated in the heterogeneous regime. *Chem. Engng Sci.* **250**, 117359.

LIEPMANN, H.W. & ROBINSON, M.S. 1953 Counting methods and equipment for mean-value measurements in turbulence research. *NACA Tech. Rep.* 3037. National Advisory Committee for Aeronautics.

MCCLURE, D.D., KAVANAGH, J.M., FLETCHER, D.F. & BARTON, G.W. 2017 Experimental investigation into the drag volume fraction correction term for gas–liquid bubbly flows. *Chem. Engng Sci.* **170**, 91–97.

MEZUI, Y., CARTELLIER, A.H. & OBLIGADO, M. 2018 Characterization of bubbles clusters in bubble column. In *Dispersed Two-Phase Flows 2018, SHF colloquium*. Toulouse, France, hal-01904598.

MEZUI, Y., CARTELLIER, A. & OBLIGADO, M. 2023 An experimental study on the liquid phase properties of a bubble column operated in the homogeneous and in the heterogeneous regimes. *Chem. Engng Sci.* **268**, 118381.

MEZUI, Y., OBLIGADO, M. & CARTELLIER, A. 2022 Buoyancy-driven bubbly flows: scaling of velocities in bubble columns operated in the heterogeneous regime. *J. Fluid Mech.* **952**, A10.

MONCHAUX, R., BOURGOIN, M. & CARTELLIER, A. 2010 Preferential concentration of heavy particles: a voronoï analysis. *Phys. Fluids* **22** (10), 103304.

MORA, D.O., ALISEDA, A., CARTELLIER, A. & OBLIGADO, M. 2018 Pitfalls measuring 1D inertial particle clustering. In *iTi Conference on Turbulence*, pp. 221–226. Springer.

MORA, D.O., ALISEDA, A., CARTELLIER, A. & OBLIGADO, M. 2019 Characterizing 1d inertial particle clustering. arXiv:1906.09896.

MORA, D.O., OBLIGADO, M., ALISEDA, A. & CARTELLIER, A. 2021 Effect of $Re\lambda$ and rouse numbers on the settling of inertial droplets in homogeneous isotropic turbulence. *Phys. Rev. Fluids* **6** (4), 044305.

NAKAMURA, K., YOSHIKAWA, H.N., TASAKA, Y. & MURAI, Y. 2020 Linear stability analysis of bubble-induced convection in a horizontal liquid layer. *Phys. Rev.* E **102** (5), 053102.

NEDELTCHEV, S. 2020 Precise identification of the end of the gas maldistribution in bubble columns equipped with perforated plate gas distributors. *Chem. Engng J.* **386**, 121535.

PANICKER, N., PASSALACQUA, A. & FOX, R.O. 2020 Computational study of buoyancy driven turbulence in statistically homogeneous bubbly flows. *Chem. Engng Sci.* **216**, 115546.

RAIMUNDO, P.M. 2015 Analyse et modélisation de l'hydrodynamique locale dans les colonnes à bulles. PhD thesis, Université Grenoble Alpes (ComUE).

RAIMUNDO, P.M., CLOUPET, A., CARTELLIER, A., BENEVENTI, D. & AUGIER, F. 2019 Hydrodynamics and scale-up of bubble columns in the heterogeneous regime: comparison of bubble size, gas holdup and liquid velocity measured in 4 bubble columns from 0.15 m to 3 m in diameter. *Chem. Engng Sci.* **198**, 52–61.

ROLLBUSCH, P., BOTHE, M., BECKER, M., LUDWIG, M., GRÜNEWALD, M., SCHLÜTER, M. & FRANKE, R. 2015 Bubble columns operated under industrially relevant conditions – current understanding of design parameters. *Chem. Engng Sci.* **126**, 660–678.

RUZICKA, M.C. 2013 On stability of a bubble column. *Chem. Engng Res. Des.* **91** (2), 191–203.

SIMONNET, M., GENTRIC, C., OLMOS, E. & MIDOUX, N. 2007 Experimental determination of the drag coefficient in a swarm of bubbles. *Chem. Engng Sci.* **62** (3), 858–866.

SUMBEKOVA, S., ALISEDA, A., CARTELLIER, A. & BOURGOIN, M. 2016 Clustering and settling of inertial particles in turbulence. In *Proceedings of the 5th International Conference on Jets, Wakes and Separated Flows (ICJWSF2015)*, pp. 475–482. Springer.

SUMBEKOVA, S., CARTELLIER, A., ALISEDA, A. & BOURGOIN, M. 2017 Preferential concentration of inertial sub-kolmogorov particles: the roles of mass loading of particles, Stokes numbers, and Reynolds numbers. *Phys. Rev. Fluids* **2** (2), 024302.

UHLMANN, M. 2020 Voronoï tessellation analysis of sets of randomly placed finite-size spheres. *Physica* A **555**, 124618.

WANG, L.-P. & MAXEY, M.R. 1993 Settling velocity and concentration distribution of heavy particles in homogeneous isotropic turbulence. *J. Fluid Mech.* **256**, 27–68.

ZUBER, N. & FINDLAY, J. 1965 Average volumetric concentration in two-phase flow systems. *Trans. ASME J. Heat Transfer* **87** (4), 453–468.